

**Separation of Alkane and Alkene by Metal-Organic Frameworks**

Journal:	<i>Journal of Materials Chemistry A</i>
Manuscript ID	TA-REV-05-2021-004096.R1
Article Type:	Review Article
Date Submitted by the Author:	19-Jul-2021
Complete List of Authors:	Wang, Hao; Shenzhen Polytechnic, Hoffmann Institute of Advanced Materials Luo, Dawei; Shenzhen Polytechnic Velasco, Ever; Rutgers University, Yu, Liang; Shenzhen Polytechnic, Hoffmann Institute of Advanced Materials Li, Jing; Rutgers The State University of New Jersey, Chemistry and Chemical Biology

# Separation of Alkane and Alkene by Metal-Organic Frameworks

Hao Wang,<sup>a#</sup> Dawei Luo,<sup>a#</sup> Ever Velasco,<sup>b</sup> Liang Yu<sup>a</sup> and Jing Li<sup>\*ba</sup>

Received 00th January 20xx,  
Accepted 00th January 20xx

DOI: 10.1039/x0xx00000x

The separation of alkane/alkene gas mixtures represents an important yet challenging process in petrochemical industry to produce valuable chemical feedstocks with sufficiently high purity. These molecules have similar physical properties, making their separation difficult and capital-intensive. The current separation and purification technology relies largely on heat-driven distillations with a huge unit composed of hundreds of trays. Adsorptive separation using porous solids is capable of accomplishing the purification at ambient conditions, offering potential energy and environmental benefits. Particularly, Metal-organic frameworks (MOFs) hold enormous promise for this separation process in light of their highly tunable pore shape, pore size, and pore surface functionality. In this review article, we provide a comprehensive account of metal-organic frameworks that have been investigated for the separation of alkane and alkene with a focus on C<sub>2</sub>-C<sub>3</sub> hydrocarbons. The material design rationale, separation mechanisms, as well as structure-property relations are highlighted. Finally, the existing challenges and possible design strategies for desirable materials are also discussed.

## 1. Introduction

The separation of light hydrocarbons into individual components with required purity remains an important goal in petrochemical industry.<sup>1, 2</sup> For example, with an annual global production over 150 million metric tons, ethylene and propylene are among the most important feedstock for manufacturing various chemical commodities, including polyethylene and polypropylene. The prime feed of ethylene and propylene come from refineries: either the by-products of steam cracking of naphtha, or off-gases from fluid catalytic cracking units. Olefins in these streams are accompanied with various impurities, in particular their corresponding alkanes, which must be removed to generate polymer-grade olefins as feedstock to produce valued polymers. Petrochemical industry currently relies on heat-driven distillations for these separations. To separate these physically similar molecules, industry relies on huge distillation units with more than a hundred trays, which inevitably consumes tremendous amounts of energy. In this context, more economical technologies, such as adsorptive separation by porous solids or membranes, are the focus of scientists and engineers in this field.

Adsorptive separation of alkane/alkene mixtures has been extensively investigated on traditional porous solids such as zeolites,<sup>3, 4</sup> activated carbons,<sup>5, 6</sup> and porous organic frameworks/polymers,<sup>7-9</sup> with zeolites as one of the most well developed classes. Various zeolites such as 13X, 4A, 5A, chabazite and ZK-5, to name a few, have been studied for the separation of propane/propylene or ethane/ethylene.<sup>3, 4, 10-12</sup> Zeolite 4A and silica chabazite (SiCHA) have been identified as the two most promising zeolite materials for the separation of propane and propylene.<sup>12, 13</sup> Detailed adsorption/separation experiments and pressure vacuum swing adsorption (PVSA)

processes have been carried out to evaluate their separation capability. While 4A requires lower separation energy per tonne of propylene compared to SiCHA, the low diffusivities limit its practical use. More recently, Corma et al. reported highly selective kinetic separation of ethane and ethylene by a flexible pure silica zeolite, ITQ-55.<sup>3</sup> Due to its structural flexibility, ITQ-55 exhibits much faster adsorption toward ethylene over ethane, with a kinetic selectivity of ~100. However, to date, no material has been widely employed for industrial alkane/alkene separation. An important factor that hinders their commercial application includes a limited pool of ideal adsorbents with high adsorption capacity and selectivity that simultaneously possess stable structures with facile scale-up synthesis. The emergence and development of metal-organic frameworks (MOFs) over the past two decades bring new opportunity for practical implementation of adsorptive separation of alkane/alkene mixtures under ambient conditions. MOFs hold particular promise for this separation process in light of their diverse structure, high surface area, and highly tunable pore structure (pore shape and pore size) and surface chemistry.<sup>14-19</sup> Tailored MOFs with optimal structure and functionality and high separation efficiency may be achievable.

Hundreds of different MOFs have been investigated for the separation of alkane/alkene mixtures over the past few years, with a bunch of them outperforming traditional adsorbents with respect to separation efficiency (adsorption capacity and selectivity).<sup>13, 20, 21</sup> The separation mechanisms mainly include thermodynamic separation, kinetic separation, and selective molecular exclusion. Additionally, some materials show separations with a high dependence on temperature or pressure, originating from structure flexibility, which may not fall into the scope of the aforementioned three types of mechanisms. MOFs that separate alkane/alkene mixtures via thermodynamic mechanism can be alkene-selective or alkane-selective. Alkene-selective MOFs commonly contain Lewis acidic moieties such as open metal sites (OMSs) that provide strong interaction with  $\pi$  bonds of alkenes. Representative examples are the MOF-74 series. It is worth noting that alkane-selective MOF materials are advantageous over alkene-

<sup>a</sup> Hoffmann Institute of Advanced Materials, Shenzhen Polytechnic, 7098 Liuxian Blvd., Nanshan District, Shenzhen, Guangdong 518055, China.

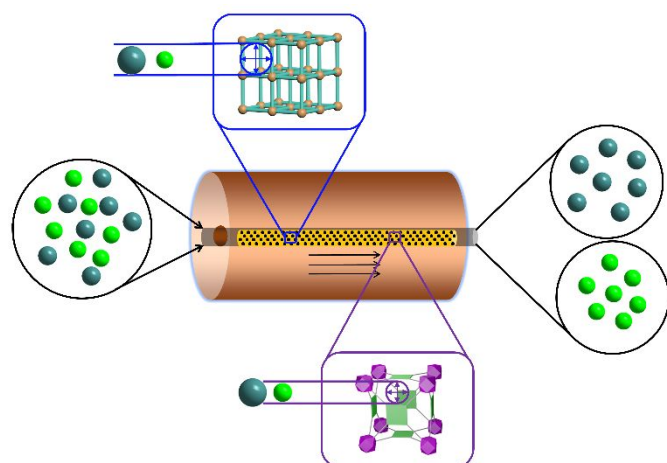
<sup>b</sup> Department of Chemistry and Chemical Biology, Rutgers University, 123 Bevier Road, Piscataway, NJ 08854, USA. E-mail: [jingli@rutgers.edu](mailto:jingli@rutgers.edu).

<sup>#</sup>These authors contributed equally to this work.

Electronic Supplementary Information (ESI) available: [details of any supplementary information available should be included here]. See DOI: 10.1039/x0xx00000x

selective analogues in removing minor alkanes from alkenes; however, alkane-selective adsorbents were previously rare and have only recently seen an influx in various reports. This group of MOFs include the well-known  $\text{Fe}_2(\text{O}_2)(\text{dobdc})$  and the newly reported NIIC-20 family. Naturally, kinetic separation is observed when MOFs show different diffusional restrictions toward alkenes and their counterpart alkanes. For example, a prototype material, ZIF-8 exhibits notable diffusional limitations for propane while propylene can enter its cages freely, leading to a propylene/propane kinetic selectivity of more than 100. Adsorbents with optimal pore structure that are capable of full separation of alkane/alkene through selective molecular exclusion are desirable for industrial implementation as such a mechanism renders infinite selectivity and high separation efficiency. This has been rarely observed for zeolites resulting from the lack of structure tunability. However, several tailor-made MOFs have achieved the separation of propane/propylene through selective molecular exclusion, including KAUST-7, Y-abtc, and Co-gallate. Such precise control of pore aperture can be attributed to the high structure tunability of MOFs and the power of reticular chemistry.

In this review article, we attempt to provide a comprehensive account of the MOFs reported to date that show potential for adsorptive separation of  $\text{C}_2\text{-C}_3$  alkane/alkene mixtures. Adsorption capacity and selectivity for these materials at ambient conditions are summarized. The compositions of alkane/alkene mixtures depend on the feed and the preceding cracking processes. Equimolar mixtures are typically used for research purposes. Ideal adsorbed solution theory (IAST) has been widely used to predict the adsorption selectivity of an adsorbent and is also summarized in this work. In most studies, experimental multicomponent column breakthrough measurements were carried out to evaluate the separation capability of the adsorbents. In addition, we focus particularly on the underlying adsorption/separation mechanism and design strategy for tailored MOF adsorbents.



**Scheme 1.** Schematic illustration of adsorptive separation by MOFs.

## 2. Thermodynamic separation

Thermodynamically-driven separation is commonly observed for MOFs and other adsorbents. This occurs when the pore size of an adsorbent is large enough to accommodate all adsorbates. Each of these individual adsorbate experiences an adsorbate-adsorbent interaction that results in preferential adsorption of adsorbates with stronger adsorption affinity. Alkene-selective adsorbents are more common in traditional inorganic and organic adsorbents, as well as in MOFs. However, a number of MOFs showing alkane-selective behavior have been developed over the past few years.

### 2.1 Alkene-selective separation

It has been well demonstrated that MOFs with OMSs preferentially interact with unsaturated hydrocarbons over their saturated counterparts, resulting in thermodynamic separation of alkane/alkene mixtures. They behave in a similar fashion to the previously known  $\pi$ -complexation adsorbents.

The first MOF with OMSs studied for alkane/alkene separation is the prototype Cu-BTC (HKUST-1,  $\text{H}_3\text{BTC} = 1,3,5\text{-benzenetricarboxylic acid}$ ). Bhatia et al. conducted quantum mechanical calculations using a Cu-tricarboxylate complex portion of Cu-BTC and investigated its adsorption toward ethylene and ethane.<sup>22, 23</sup> The results indicated that at low loadings ethylene was favored as a result of its strong electrostatic interactions with the framework, leading to an ethylene/ethane selectivity of 2. However, the selective adsorption was weakened at higher loadings due to the stronger van der Waals affinity of ethane with the complex. In a subsequent study, Wang et al. performed Grand canonical Monte Carlo (GCMC) simulations of adsorption and separation of ethylene/ethane mixtures on Cu-BTC.<sup>24</sup> The ethylene/ethane selectivity was calculated to be 2, which is consistent with the previous results. Nevertheless, a decrease of selectivity as an increase in pressure was not observed in this GCMC calculation. Experimental evaluation of alkane/alkene separation by Cu-BTC were carried out by Limia et al. and Yoon et al. Preferential adsorption of propylene over propane was observed with higher adsorption capacity and isosteric heat.<sup>25</sup> Very recently, Wu et al. developed a functionalized Cu-BTC material,  $\text{Pyr}_{1/3}\text{@Cu-BTC}$ , by grafting pyrrole molecules onto the open Cu sites of the framework.<sup>26</sup> Separation capability of propylene and propane by this material was evaluated and compared to its parent structure. The results suggested that the functionalized MOF show enhanced adsorption capacity and selectivity.  $\text{Pyr}_{1/3}\text{@Cu-BTC}$  exhibited a notably high adsorption capacity of 7.6 mmol/g for propylene at 298 K and 1 bar, higher than that of the pristine Cu-BTC (7.0 mmol/g). In addition, an increase of IAST propylene/propane selectivity from 4.1 to 5.5 for an equimolar binary mixture was observed upon pyrrole functionalization. Its capability for the separation of propane and propylene was confirmed by multicomponent column breakthrough measurements. More importantly, the grafted pyrrole molecules protected the Cu sites from being attacking

by H<sub>2</sub>O, leading to largely enhanced moisture stability of the functionalized material. This study indicated that judicious functionalization on OMSs of a MOF with optimal loading may simultaneously enhance its olefin/paraffin separation efficiency and structural stability towards water.

Another MOF with OMSs that was examined for alkane/alkene separation at the early stage of this research field was MIL-100(Fe). The study was carried out by Serre et al. in 2010.<sup>27</sup> MIL-100(Fe) is built on  $\mu_3$ -oxo-centered trimers of Fe<sup>III</sup> octahedra where two out of three iron octahedra have terminal H<sub>2</sub>O molecules that can be removed upon heating leading to the exposure of open Fe<sup>III</sup> sites (activation at 100 °C) or a mixture of Fe<sup>II</sup> and Fe<sup>III</sup> sites (activation at 250 °C). Adsorption measurements of propane and propylene were performed on both samples (activated at 100 °C and 250 °C) and the results indicated that the presence of Fe<sup>II</sup> dramatically enhanced the adsorption affinity toward propylene and propylene/propane selectivity at low pressure. Open Fe<sup>III</sup> sites are also effective in

the preferential adsorption of propylene over propane however their interaction with propylene is weakened compared to that of Fe<sup>II</sup>. The authors attributed this to the presence of an additional d electron in the iron(II) orbitals leading to a  $\pi$  backbonding interaction with propylene. The feasibility of using MIL-100(Fe) for the separation of propane and propylene was confirmed by breakthrough tests with equimolar propane/propylene binary mixtures. Their results show that a column packed with a 250 °C activated sample can elute propane out at the 7<sup>th</sup> minute while propylene was retained in the column for 175 minutes, indicating a clear separation between the two gases. A propylene/propane separation factor of 28.9 was calculated from the breakthrough results at low pressure. This value was substantially higher than that for Cu-BTC in the previous studies. However, a pronounced decrease in the separation factor was observed with increasing partial pressure of the gas mixture resulting from the involvement of Fe<sup>III</sup>.

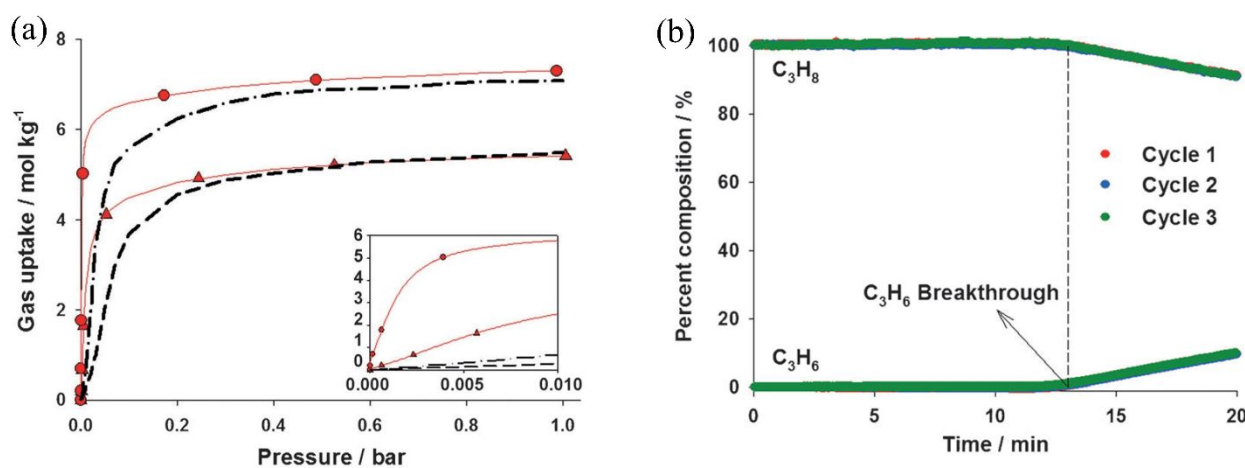


**Figure 1.** a) Adsorption isotherms for C<sub>3</sub>H<sub>6</sub> (circles) and C<sub>3</sub>H<sub>8</sub> (triangles) in Co-MOF-74 at 298 K. The inset shows the low-pressure isotherms. Solid lines through the experimental data are fits of the dual-site Langmuir–Freundlich model. b) Breakthrough curves of equimolar mixtures of propene and propane (total flow rates=30 mL min<sup>-1</sup>) in a packed column of Co-MOF-74 that is initially saturated with C<sub>3</sub>H<sub>8</sub>. These curves were obtained for three consecutive cycles after the column had been regenerated by flowing pure propane. Reproduced with permission.<sup>28</sup> Copyright 2012, Wiley-VCH.

The MOF-74-M (M = Zn, Fe, Co, Ni, Mn, Mg, etc.) family represent the most extensively studied materials in this category. This family of materials can be easily synthesized through solvothermal reactions with H<sub>4</sub>DOBDC (2,5-dihydroxyterephthalic acid) and the corresponding metal nitrate in DMF-ethanol-water mixed solvent with relatively high yield. Bao et al. carried out the first study of alkane/alkene separation with materials in this family.<sup>29</sup> With combined experimental exploration and GCMC simulation, the authors investigated the adsorption and separation of ethane, ethylene, propane, and propylene on MOF-74-Mg. As expected, the compound showed favoured adsorption toward propylene and ethylene over propane and ethane, with higher adsorption capacity and stronger affinity for the former. GCMC simulation revealed all four adsorbate molecules are preferentially

adsorbed on the open Mg sites but with stronger interaction for alkenes. It is noteworthy that the material demonstrated higher adsorption affinity to propylene and propane than that of ethane and ethylene, which should be attributed to the significant dipole moments of the former. In an independent study carried out almost at the same time, Bae et al. evaluated the performance of MOF-74-M (M= Co, Mn, and Mg) for the separation of propane and propylene.<sup>28</sup> All three compounds showed selective adsorption of propylene over propane, as evidenced by single-component gas adsorption experiments and multicomponent column breakthrough measurements (Figure 1). However, propylene/propane selectivity was found to be highly dependent on metal species in this series of MOFs, and the values followed the order of Co > Mn > Mg. MOF-74-Co showed an IAST selectivity of 46 for an equimolar binary mixture

at 298 K and 1 bar, notably higher than that of MIL-100(Fe), the previous record holder. The underlying reason was explored by first-principle calculations for the binding energies between propylene/propane and all three compounds. It was revealed that MOF-74-Co had the highest binding energy towards propylene compared to the other two analogues. Additionally, it also showed the largest difference between binding energies for propylene and propane leading to the highest propylene/propane selectivity. Interestingly, different trends of alkene/alkane selectivity as a function of pressure were observed by the authors for MOF-74-Co. The selectivity of

propylene/propane increased as pressure increased while for ethylene/ethane the trend was reversed. The authors attributed this to the proper match of the pore size and the size of propane/propylene molecules, leading to competitive adsorption between propane and propylene to the OMSs as pressure increased. In contrast, a considerable amount of pore volume was left for the adsorption of additional ethane or ethylene after the OMSs were occupied mainly by ethylene molecules and thus ethylene/ethane selectivity decreased as pressure increased.

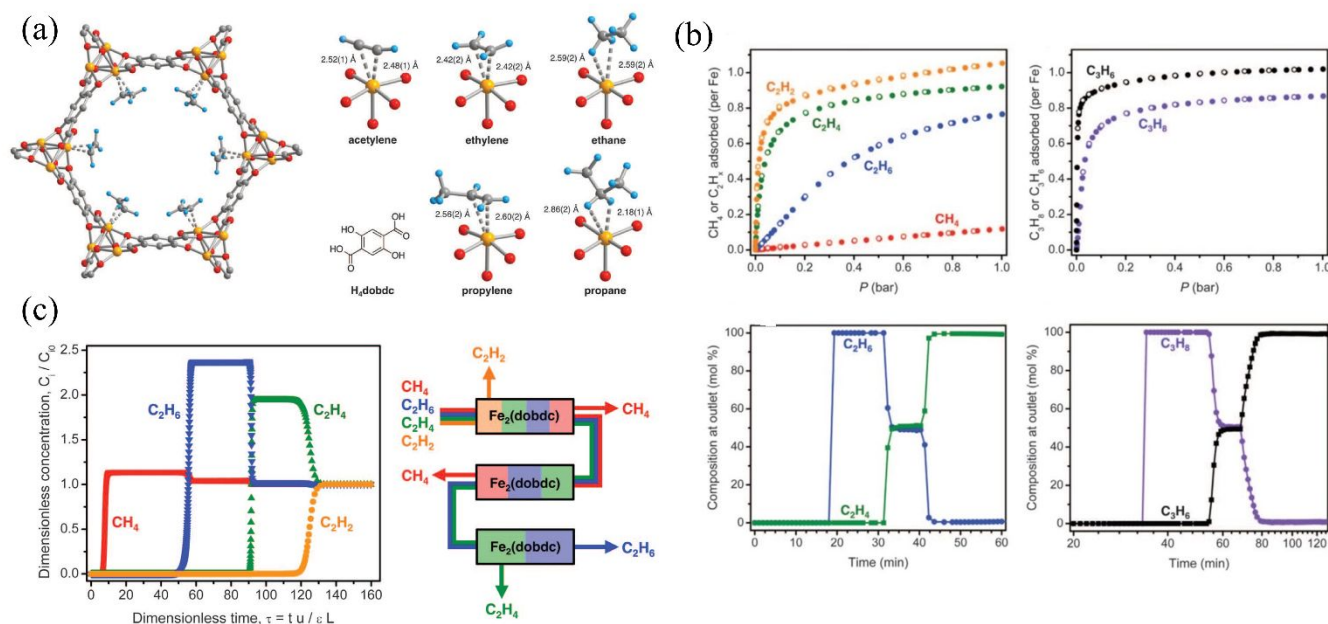


**Figure 2.** a) (Left) A portion of the solid-state structure of Fe<sub>2</sub>(dobdc)·2C<sub>2</sub>D<sub>4</sub> as determined by analysis of neutron powder diffraction data; orange, red, gray, and blue spheres represent Fe, O, C, and D atoms, respectively. (Right) H<sub>4</sub>(dobdc) ligand and the first coordination spheres for the iron centers in the solid-state structures obtained upon dosing Fe<sub>2</sub>(dobdc) with acetylene, ethylene, ethane, propylene, and propane. b) (Top) Gas adsorption isotherms for methane, ethane, ethylene, and acetylene and propane and propylene in Fe<sub>2</sub>(dobdc) at 318 K. Filled and open circles represent adsorption and desorption data, respectively. (Bottom) Experimental breakthrough curves for the adsorption of equimolar ethane/ethylene and propane/propylene mixtures flowing through a 1.5-mL bed of Fe<sub>2</sub>(dobdc) at 318 K with a total gas flow of 2 mL/minute at atmospheric pressure. c) (Left) Calculated methane (red), ethane (blue), ethylene (green), and acetylene (orange) breakthrough curves for an equimolar mixture of the gases at 1 bar flowing through a fixed bed of Fe<sub>2</sub>(dobdc) at 318 K. (Right) Schematic representation of the separation of a mixture of methane, ethane, ethylene, and acetylene using just three packed beds of Fe<sub>2</sub>(dobdc) in a vacuum swing adsorption or temperature swing adsorption process. Reproduced with permission.<sup>30</sup> Copyright 2012, AAAS.

In another work reported simultaneously, Long et al. carried out an in-depth investigation of alkane/alkene adsorption and separation on MOF-74-Fe,<sup>30</sup> which has a higher surface area and softer metal character compared to its analogues in previous studies (Figure 2). Single-component adsorption results indicated that the uptake amounts of ethylene and propylene were approaching one molecule per iron(II) center at 313 K and 1 bar, while the adsorbed amounts of ethane and propane were notably lower, particularly at low pressure region. Neutron powder diffraction analysis confirmed that open iron(II) centers in the structure of MOF-74-Fe were the primary binding sites for

alkenes. Ethylene and propylene interact with iron(II) through side-on binding modes, with Fe-C distances of 2.42 and 2.56 Å, respectively. Column breakthrough measurements displayed that the material was capable of separating ethylene/ethane and propylene/propane mixtures into individual components with 99%+ purity. IAST adsorption selectivity of ethylene/ethane for MOF-74-Fe was calculated to be 13 to 18 at 318 K, higher than zeolite NaX and its isostructural Mg analogue as a result of the softer character of Fe(II) relative to Mg(II), leading to a stronger interaction between alkene molecules and the former. To further evaluate alkene/alkane

separation capability of MOF-74-Fe and compare it with other adsorbents, the authors carried out simulated breakthrough modelling. The amount of polymer-grade (99.5%+) propylene that can be produced was calculated from simulated breakthrough curves for MOF-74-Fe and a series of reported materials. The results indicated that MOF-74-Fe showed a higher propylene/propane separation efficiency than that of all other zeolites and MOFs, including ITQ-12, NaX, Cu-BTC, Cr-BTC, MIL-100-Fe, and MOF-74-Mg. This should be attributed to the fact that MOF-74-Fe has both high alkene/alkane selectivity and high adsorption capacity. Evaluation for ethylene/ethane mixtures also indicates that MOF-74-Fe outperformed other adsorbents studied.

In a subsequent study, Long et al. performed a systematic evaluation of alkane/alkene separation for the entire series of

MOF-74-M (M = Mg, Mn, Fe, Co, Ni, Zn).<sup>31</sup> The adsorption capacity and selectivity of these materials is closely related to the metal species. IAST calculations from experimental isotherms indicated that MOF-74-Fe and MOF-74-Mn had the highest selectivities for ethylene/ethane and propylene/propane, respectively. In contrast, the Mg and Zn analogues exhibited the lowest selectivities for both separations, which was attributed to the weaker affinities of these metals to olefins. This was confirmed by the isosteric heats of adsorption ( $Q_{st}$ ) where MOF-74-Fe and MOF-74-Mn had the highest value for ethylene and propylene, respectively while the Mg and Zn analogues showed the lowest value for the two olefins.

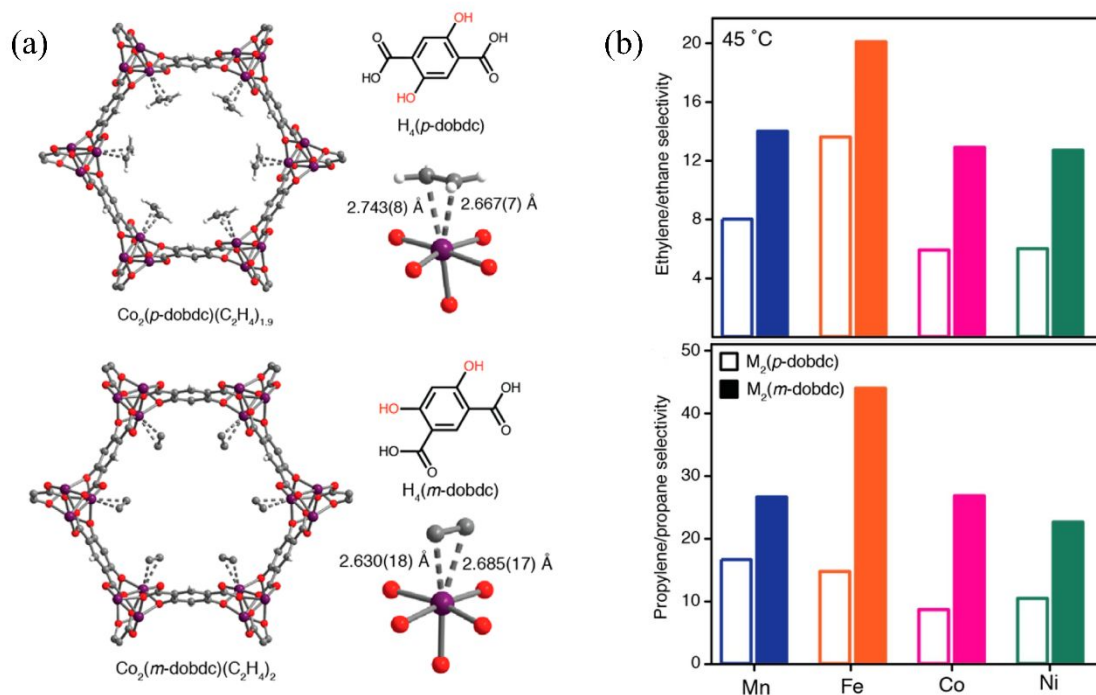


**Figure 3.** a) Comparison of the framework structures, ligand structure, and ethylene binding geometries for (Top)  $\text{Co}_2(\text{p-dobdc})$  and (Bottom)  $\text{Co}_2(\text{m-dobdc})$  under  $\sim 0.3$  bar of ethylene at 100 K as determined from *in situ* single-crystal X-ray diffraction experiments. Purple, red, gray, and white spheres represent Co, O, C, and H atoms, respectively. b) Comparison of the IAST selectivity under an equimolar feed at 45 °C between  $\text{M}_2(\text{p-dobdc})$  and  $\text{M}_2(\text{m-dobdc})$  (M = Mn, Fe, Co, Ni) for (Top) ethylene/ethane and (Bottom) propylene/propane separations. Reproduced with permission.<sup>32</sup> Copyright 2017, American Chemical Society.

Inspired by the excellent performance of MOF-74-M ( $\text{M}_2(\text{p-dobdc})$ ) for the separation of alkane/alkene mixtures, Long et al. developed a new series of MOFs built on *m-dobdc* in order to alter the affinity of the OMSs and their olefin/paraffin selectivities.<sup>32</sup> The new materials can be prepared in gram scale by stirring a mixture of  $\text{H}_4(\text{m-dobdc})$  and the corresponding metal chloride in DMF under heating. The formed  $\text{M}_2(\text{m-dobdc})$  (M=Mg, Mn, Fe, Co, Ni) feature isostructures to MOF-74-M. Experimental results indicated that  $\text{M}_2(\text{m-dobdc})$  exhibited markedly enhanced alkene/alkane selectivities compared to

their *para*-functionalized counterparts (Figure 3). In particular,  $\text{Fe}_2(\text{m-dobdc})$  showed ethylene/ethane and propylene/propane selectivities of 25 and 55, respectively. This was attributed to the higher charge density at the metal sites in the *meta*-substituted variants leading to stronger adsorption affinity to alkenes compared to their *para*-substituted isomers. The hypothesis was experimentally confirmed by *in situ* single-crystal X-ray diffraction analysis of ethylene adsorbed crystals which showed a shorter Co-C distance in  $\text{Co}_2(\text{m-dobdc})$  than that in  $\text{Fe}_2(\text{p-dobdc})$ . The selective adsorption of alkene over

alkane on  $M_2(m\text{-dobdc})$  resulted from the preferential adsorption of alkene molecules on OMSs, similar to that for  $M_2(p\text{-dobdc})$ . Expected side-on interactions between alkenes and OMSs in  $M_2(m\text{-dobdc})$  were also experimentally observed. The combined features of high adsorption capacity and selectivity, fast adsorption kinetics, and relatively low cost make  $M_2(m\text{-dobdc})$  promising adsorbents for alkene/alkane separations. The authors concluded that the material design strategy employed in this work may be generalized and that tuning the electronic environment around a given adsorption site in a given structure may largely affect adsorption and separation properties.

Besides OMSs formed intrinsically in MOF structures, metal binding sites which are added post-synthetically to the materials may also play an important role in favoured adsorption of alkenes over alkanes. Bao et al. reported the immobilization of Ag(I) into sulfonic acid functionalized MIL-101(Cr) to form MIL-101(Cr)-SO<sub>3</sub>Ag.<sup>33</sup> MIL-101(Cr)-SO<sub>3</sub>Ag was easily obtained by stirring a mixture of MIL-101(Cr)-SO<sub>3</sub>H and AgBF<sub>4</sub> in a mixed solvent of CH<sub>3</sub>CN/H<sub>2</sub>O. The Ag(I) loaded compound showed a suppressed BET surface area of 1253 m<sup>2</sup>/g compared to that of the pristine MIL-101(Cr)-SO<sub>3</sub>H (1856 m<sup>2</sup>/g). However, the adsorption capacities of ethylene and propylene were noticeably enhanced upon Ag(I) loading particularly at low pressure region indicating strong interactions between Ag(I) and alkene molecules. This was confirmed by the isosteric heats of adsorption results. The  $Q_{st}$  of ethylene and propylene in MIL-101(Cr)-SO<sub>3</sub>H were 35 and 41 kJ/mol while the values for MIL-101(Cr)-SO<sub>3</sub>Ag were calculated to be 120 and 101 kJ/mol, which are comparable to the binding energies in Ag(I)-based  $\pi$ -complexation systems. This indicated the substantially enhanced affinity toward alkenes in MIL-101(Cr)-SO<sub>3</sub>Ag should originate from the  $\pi$ -complexation between alkene molecules and the loaded Ag(I) ions. The enhanced interactions to alkenes in MIL-101(Cr)-SO<sub>3</sub>Ag led to its notably improved alkene/alkane selectivity. IAST selectivity of ethylene/ethane increased from 1.15 for MIL-101(Cr)-SO<sub>3</sub>H to 16 for its Ag(I) loaded analogue. Similar strategy was also effectively applied to other adsorbents such as porous aromatic frameworks.<sup>9</sup>

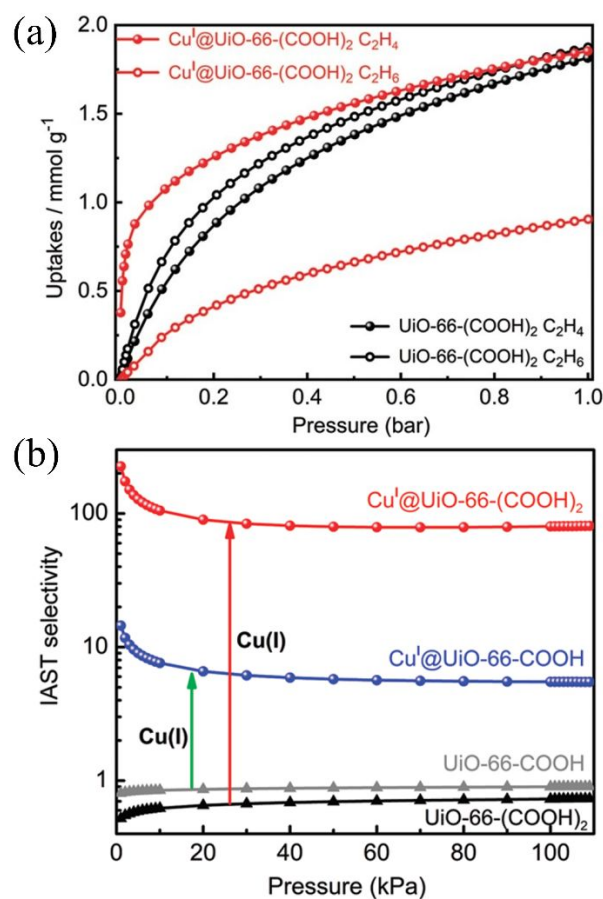


**Figure 4.** a) Single-component adsorption isotherms for C<sub>2</sub>H<sub>4</sub> and C<sub>2</sub>H<sub>6</sub> of UiO-66-(COOH)<sub>2</sub> and Cu'@UiO-66-(COOH)<sub>2</sub> at 298 K. b) IAST calculations of activated UiO-66-type MOFs for the C<sub>2</sub>H<sub>4</sub>/C<sub>2</sub>H<sub>6</sub> separation at 298 K. Reproduced with permission.<sup>34</sup> Copyright 2020, Wiley-VCH.

In a more recent study,<sup>34</sup> Qian et al. developed Cu'@UiO-66-(COOH)<sub>2</sub> with optimal pore window size and chelated Cu(I) ions that forms  $\pi$ -complexation with ethylene (Figure 4). The loading of Cu(I) was carefully carried out in a glovebox under inert atmosphere by stirring CuCl and the parent material in acetonitrile. The authors systematically investigated the evolution of surface area, pore size, and ethylene/ethane separation properties from UiO-66-COOH and UiO-66-(COOH)<sub>2</sub> to Cu'@UiO-66-(COOH) and Cu'@UiO-66-(COOH)<sub>2</sub>. The loading of -COOH functional groups and Cu(I) ions not only offer strong adsorption sites for ethylene, but also tune the pore aperture so that ethylene was optimally adsorbed while ethane was partially excluded in Cu'@UiO-66-(COOH)<sub>2</sub>. This led to an exceptionally high ethylene/ethane selectivity of 80.8 in Cu'@UiO-66-(COOH)<sub>2</sub>, outperforming most previously described benchmark adsorbents.

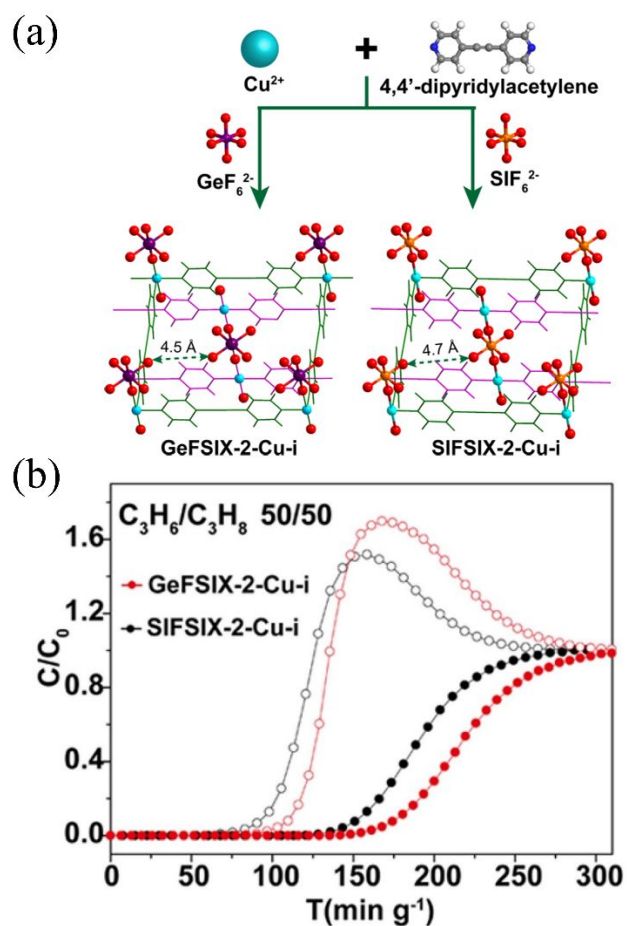


**Figure 5.** a) Structures of  $\text{GeFSIX-2-Cu-i}$  and  $\text{SIFSIX-2-Cu-i}$ . Color code: F, red; N, blue; Cu, Indigo; Ge, purple; Si, yellow; H, light gray; C, green/rose red (the different nets are highlighted in green and rose red for clarity). b) Breakthrough tests for  $\text{C}_3\text{H}_6/\text{C}_3\text{H}_8$  (50/50, v/v) at 298 K and 1 bar carried out on  $\text{GeFSIX-2-Cu-i}$  and  $\text{SIFSIX-2-Cu-i}$ . Reproduced with permission.<sup>35</sup> Copyright 2020, American Chemical Society.

MOFs without OMSs or additional metal binding sites may also be capable of selectively adsorbing alkenes over alkanes through soft supramolecular interactions. The representative MOF in this category is NOTT-300 reported by Yang et al.<sup>36</sup> NOTT-300 is built on one-dimensional (1D)  $[\text{AlO}_4(\text{OH})_2]$  chains bridged by biphenyl-3,3',5,5'-tetracarboxylate ( $\text{bptc}^{4-}$ ) linkers affording three-dimensional (3D) porous structure possessing 1D channels with a diameter of 6.5 Å. The compound has a BET surface area of 1370  $\text{m}^2/\text{g}$ . It adsorbed 4.28  $\text{mmol}/\text{g}$  of ethylene at 293 K and 1 bar, which was substantially higher than that for ethane (0.85  $\text{mmol}/\text{g}$ ) under identical conditions. The great difference in the uptakes between ethylene and ethane in NOTT-300 led to a remarkably high ethylene/ethane selectivity of 48.7, exceeding the values for adsorbents reported prior to this work. Combined exploration by *in situ* synchrotron X-ray and neutron powder diffraction, inelastic neutron scattering (INS), and DFT calculations revealed that ethylene exhibited a

side-on interaction with the HO-Al group via hydrogen bonding and  $\pi\cdots\pi$  stacking interactions to the phenyl rings. In comparison, the adsorbed ethane molecules were aligned at a very long distance to the -OH groups because of an absence of  $\pi$ -electron density and repulsion between the hydrogen atoms, leading to its weaker interaction with the framework compared to ethylene. This study indicated that the relatively weak supramolecular bonding interactions in MOFs may be sufficiently strong to selectively adsorb alkene over alkane with high adsorption selectivity.

Anion-pillared MOFs have been extensively studied for the separation of alkyne/alkene as well as alkene/alkane mixtures. Cui et al. reported the separation of propylene and propane by two isostructural anion-pillared MOFs,  $\text{GeFSIX-2-Cu-i}$  and  $\text{SIFSIX-2-Cu-i}$  (Figure 5).<sup>35</sup> Both materials showed selective adsorption of propylene over propane, originating from the strong hydrogen-bonding interactions between  $\text{GeF}_6^{2-}/\text{SiF}_6^{2-}$  anions and propylene in addition to  $\pi$ - $\pi$  interactions between the organic linkers and  $\text{C}_3\text{H}_6$ . The extent of adsorption affinity was characterized by isosteric heats of adsorption.  $\text{GeFSIX-2-Cu-i}$  showed a  $Q_{st}$  of 35.8  $\text{kJ}/\text{mol}$  for propylene, notably higher than that for propane (20.4  $\text{kJ}/\text{mol}$ ). It is noteworthy that these values are lower compared to MOFs with OMSs or other stronger adsorption sites and may be beneficial for material regeneration in practical implementation.

Flexible MOFs represent a unique family of materials that usually show unexpected adsorption behaviors toward various guest molecules. This can sometimes be beneficial for applications relating to gas storage and separation. Structural flexibility of MOFs may be selectively utilized for the separation of alkene/alkane mixtures. Since structure transformations of MOFs relate to the extent of host-guest interactions, we will discuss these within thermodynamically-driven separation category. Li et al. reported the separation of propane and propylene in a flexible MOF, NJU-Bai8, through its guest-dependent, pressure induced gate-opening effect.<sup>37</sup> NJU-Bai8 is built on paddle-wheel  $\text{Cu}_2(\text{COO})_4\text{N}_2$  SBUs bridged by 5-(pyrimidin-5-yl) isophthalate linkers forming 3D structure with 1D channels. The dumbbell-like channels are decorated with bulging pyrimidine rings that swell upon guest inclusion and removal thus resulting in structural flexibility. Adsorption profiles of propylene and propane were characterized by "S" shaped curves which are commonly observed for flexible MOFs. There is essentially no uptake before gate-opening pressure while after the threshold pressure the adsorption rapidly reaches saturation. For a given temperature, the gate-opening pressure for propylene is notably lower than that of propane, indicating stronger interaction between the former and the framework. The difference in gate-opening pressures for propylene and propane can be utilized for the separation of these two gases, and the feasibility was confirmed by experimental column breakthrough measurements.

With synergistic sorbent separation technology (SSST), Zaworotko et al. achieved one-step ethylene purification from

a four component mixture including ethylene, ethane, acetylene, and carbon dioxide.<sup>38</sup> A series of different adsorbents were packed in a single column to enhance the separation efficiency for multicomponent gas mixtures. For example, a three-component sorbent bed was used to separate a four-component equimolar mixture of C<sub>2</sub>H<sub>2</sub>/C<sub>2</sub>H<sub>4</sub>/C<sub>2</sub>H<sub>6</sub>/CO<sub>2</sub>.

Column breakthrough measurements indicated that CO<sub>2</sub>, C<sub>2</sub>H<sub>6</sub>, and C<sub>2</sub>H<sub>2</sub> were preferentially captured so that C<sub>2</sub>H<sub>4</sub> eluted out with polymer-grade purity. The SSST strategy may be generalized and the adsorbents can be optimized to achieve highly selective separation toward specific gas mixtures.

Table 1. Representative MOFs showing thermodynamic separation for alkane/alkene

MOF	BET surface area (m <sup>2</sup> /g)	Aperture size (Å)	Uptake (mmol/g)		Selec.	Temp. (K)	Ref.
			alkene	alkane			
Propylene-selective							
MOF-74-Fe	1536	11	6.9	6.2	14.7	318	39
MOF-74-Mg	1835	11	7.5	6.0	5.5	318	29, 31
MOF-74-Mn	1797	11	7.2	6.0	16.6	318	31
MOF-74-Co	1438	11	6.8	5.9	8.6	318	31
MOF-74-Ni	1532	11	7.0	5.7	10.4	318	31
MOF-74-Zn	1277	11	6.3	5.5	3.9	318	31
MIL-101-Cr-SO <sub>3</sub> H	1856	15	4.5	3.8	1.1	303	33
MIL-101(Cr)-SO <sub>3</sub> H-Ag	1253	15	4.3	3.0	6.0	303	33
ZIF-4	300	4.9	2.4	2.4	1.1	293	40
Mn <sub>2</sub> (m-dobdc)	/	/	7.5	6.0	40	298	32
Fe <sub>2</sub> (m-dobdc)	/	/	7.5	6.0	52	298	32
Co <sub>2</sub> (m-dobdc)	/	/	7.5	6.0	39	298	32
Ni <sub>2</sub> (m-dobdc)	/	/	7.5	6.0	35	298	32
Cu@MIL-100(Fe)	1490	5.5	3.4	2.2	34	323	41
Zn <sub>2</sub> (5-aip) <sub>2</sub> (bpy)	/	8.1	1.9	0.7	20	298	42
NJU-Bai8	1048	/	2.8	2.8	4	298	37
MIL-101(Cr)-DAA	3501	/	7.5	6.5	2	303	43
AGTU-3a	227	/	1.2	0.5	7	298	44
GeFSIX-2-Cu-i	/	4.5	2.7	1.6	4.0	298	35
Pyr <sub>1/3</sub> @Cu-BTC	1510	8.5	7.0	6.7	5.5	298	26
Propane-selective							
WOFOUR-1-Ni	/	5.6	1.2	1.0	1.6	298	45
BUT-10	1726	/	6.3	5.8	1.4	298	46
Zr-BPDC	2094	11	8.8	8.4	1.2	298	47
g-C <sub>3</sub> N <sub>4</sub> @Zr-BPDC	2409	11	8.9	8.9	1.4	298	47
Zr-BPYDC	2080	12	6.8	7.2	1.6	298	47
ZIF-8	1844	3.4	4.5	4.6	1.3	298	48
Ethylene-selective							
MOF-74-Fe	1536	11	6.3	5.2	13.6	318	30, 31
MOF-74-Mg	1835	11	6.2	4.8	4.4	318	29, 31
MOF-74-Mn	1797	11	6.3	5.2	8.1	318	31
MOF-74-Co	1438	11	6.2	5.3	5.8	318	31
MOF-74-Ni	1532	11	6.0	4.7	5.9	318	31
MOF-74-Zn	1277	11	5.4	4.6	2.7	318	31
MIL-101-Cr-SO <sub>3</sub> H	1856	15	1.7	1.6	1.2	303	33
MIL-101-Cr-SO <sub>3</sub> H-Ag	1253	15	2.6	1.2	16	303	33
ZIF-4	300	4.9	2.3	2.2	2.0	293	40
Mn <sub>2</sub> (m-dobdc)	/	/	6.8	6.1	17	298	32
Fe <sub>2</sub> (m-dobdc)	/	/	7.0	6.2	25	298	32
Co <sub>2</sub> (m-dobdc)	/	/	7.0	6.2	15	298	32
Ni <sub>2</sub> (m-dobdc)	/	/	6.6	6.0	16	298	32
MIL-101	2892	/	4.0	2.9	0.8	303	49
MIL-101-6Cu	1680	/	4.5	2.0	12.5	303	49
MIL-101-6Ni	2110	/	4.3	2.4	1.2	303	49
CPL-2	/	/	2.9	2.8	1.5	298	50

Journal Name							ARTICLE
Ag/CPL-2	/	/	0.9	0.2	25	298	50
1.6AgM-DS	846	/	3.4	1.0	9.5	298	51
Cu <sup>1</sup> @UiO-66-COOH	437	4.5	1.4	0.9	5.5	298	34
Cu <sup>1</sup> @UiO-66-(COOH) <sub>2</sub>	319	4.1	1.9	0.9	80.8	298	34
NUS-36	298	3.5	1.5	1.0	4.1	298	52
Ca(squarate)	224	3.4	2.3	1.3	5.9	298	53
NUS-6(Hf)-Ag	1027	/	2.0	1.3	6.0	298	54
Ethane-selective							
DUT-8(Cu)	2370	/	1.9	3.4	1.4	303	55
DUT-8(Ni)	2440	/	2.3	4.0	1.7	303	55
CPM-80-Zn	995	13.3	4.2	4.7	1.8	298	56
CPM-80-Co	895	13.3	3.8	4.2	1.8	298	56
CPM-80-Fe	862	13.3	4.0	4.5	1.8	298	56
CPM-81-Zn	907	13.3	4.1	4.4	1.8	298	56
CPM-81-Co	1020	13.3	5.1	5.4	1.8	298	56
CPM-82-Zn	568	13.3	3.5	4.0	1.6	298	56
NIIC-20-Et	1161	~ 25	1.8	2.4	3.5	298	57
NIIC-20-Pr	1117	~ 25	1.9	2.4	4.0	298	57
NIIC-20-Bu	1033	~ 25	1.4	2.5	15.4	298	57
NIIC-20-Pe	1023	~ 25	1.6	2.2	8.4	298	57
NIIC-20-Gl	963	~ 25	1.7	2.1	8.7	298	57
MUF-15	1130	3.6	4.1	4.6	2.0	293	58, 59
MUF-15-F	874	3.4	2.9	3.2	1.1	293	58
MUF-15-Br	734	3.3	2.1	2.0	1.3	293	58
MUF-15-NO <sub>2</sub>	762	/	2.7	2.5	0.4	293	58
MUF-15-CH <sub>3</sub>	967	3.5	2.6	2.7	1.6	293	58
Ca(H <sub>2</sub> tcpb)	200	5.5	2.7	2.8	2.0	298	60
Ni1-a	1474	5.5	5.2	5.9	1.6	298	61
CPM-63m	1023	/	2.5	2.9	1.5	298	62
Y-BTC	933	/	3.1	3.5	1.9	298	63
Sm-BTC	700	/	1.6	1.7	1.8	298	63
Eu-BTC	720	/	2.8	3.1	1.9	298	63
Dy-BTC	947	/	1.9	1.9	1.4	298	63
Mn-PNMI	818	13.3	2.0	2.7	1.4	298	64
Zn-PNMI	305	/	1.5	1.6	1.4	298	64
Cd-PNMI	264	/	1.4	1.9	1.3	298	64
Cu(Qc) <sub>2</sub>	240	/	2.0	0.8	3.4	298	65, 66
RT-Cu(Qc) <sub>2</sub>	251	/	0.6	2.2	4.1	298	65
NUM-7a	345	3.4	2.7	2.9	1.7	298	67
NJU-120	1597	4.4	3.9	4.9	2.7	296	68
Cr-BTC(O <sub>2</sub> )	1135	/	2.9	3.3	1.5	298	69
CPM-733	1328	7.3	6.3	7.1	1.7	298	70
CPM-736	472	5.9	3.9	4.0	1.6	298	70
CPM-738	1161	5.9	4.6	4.7	1.4	298	70
CPM-723	1369	6.8	6.7	6.9	1.5	298	70
CPM-223(Ti)	1460	6.8	6.3	6.9	1.6	298	70
CPM-223-tpy	1599	6.8	7.3	7.2	1.3	298	70
CPM-223-tpbz	1661	6.8	6.2	6.9	1.5	298	70
CPM-223(V)	1597	6.8	6.5	7.4	1.6	298	70
Ni(bdc)(ted) <sub>0.5</sub>	1905	5.8	3.3	4.8	1.6	298	71, 72
Zn(bdc)(ted) <sub>0.5</sub>	1781	5.8	3.2	4.5	1.5	298	71
Co(bdc)(ted) <sub>0.5</sub>	1708	5.8	2.8	4.1	1.6	298	71
Cu(bdc)(ted) <sub>0.5b</sub>	1631	5.9	2.5	3.7	1.6	298	71
JNU-2	1219	3.7	3.5	4.1	/	298	73
Zr-bptc	1085	5.0	3.1	3.3	1.4	298	74
UiO-66-2CF <sub>3</sub>	467	/	1.5	1.8	2.3	298	75
Ni-4PyC	945	5.0	3.5	3.8	1.7	298	76
Ni(BDC)(DABCO) <sub>0.5</sub>	2050	8.6	3.1	4.3	1.6	298	77
Ni(BDC) <sub>0.8</sub> (TMBDC) <sub>0.2</sub> (DABCO) <sub>0.5</sub>	1556	8.0	4.0	4.9	1.7	298	77

## REVIEW

## Journal Name

Ni(BDC) <sub>0.55</sub> (TMBDC) <sub>0.45</sub> (DABCO) <sub>0.5</sub>	1294	8.0	4.3	5.0	1.7	298	77
Ni(BDC) <sub>0.29</sub> (TMBDC) <sub>0.71</sub> (DABCO) <sub>0.5</sub>	1084	7.3	4.8	5.5	1.9	298	77
Ni(TMBDC)(DABCO) <sub>0.5</sub>	894	5.9	5.0	5.4	2.0	298	77
In-soc-MOF-1	1223	6.8	3.7	4.0	1.4	298	78
UiO-66-ADC	556	4.4	1.7	1.6	1.8	298	52
MIL-53(Al)-FA	1160	6.0	3.8	3.9	1.8	298	60
Fe <sub>2</sub> (O <sub>2</sub> )(dobdc)	1073	/	2.5	3.3	4.4	298	20
MIL-142A	1555	10	2.9	3.8	1.5	298	79
PCN-245	1743	10	2.4	3.3	1.8	298	80
PCN-250	1470	5.9	4.2	5.2	1.8	298	81
ZIF-69	882	/	1.8	2.2	1.7	298	82
MAF-49	/	/	1.7	1.7	2.7	316	83
IRMOF-8	1360	12.6	3.1	4.1	1.8	298	84

Notes: (1) Gas uptakes were measured at the specified temperature and 1 bar. (2) Selectivities were calculated using the IAST model.

## 2.2 Alkane-selective separation

Most of the reported porous materials for alkene/alkane separation, including zeolites, metal oxides, and MOFs, show alkene-favored behavior. This could be attributed to the stronger interaction between alkene molecules and metal centers/clusters through  $\pi$ -complexation. We have also presented in the foregoing examples that without metal binding sites MOFs may also show selective adsorption of alkene over alkane through supramolecular interactions such as  $\pi$ - $\pi$  stacking. However, since alkenes are the favored components in alkene/alkane separation, an additional desorption step is needed if alkene-selective adsorbents are employed. In comparison, alkane-selective adsorbents would be more desirable, particularly in the cases where minor alkane impurities need to be removed from alkene, as they produce high-purity alkene directly during the adsorption step. This would make the separation scheme much simpler and efficient. It has been proposed that nonpolar/inert surfaces such as aromatic or aliphatic moieties are important features for alkane-selective adsorbents. A number of MOFs which selectively adsorb alkane over alkene have been reported over the past few years.

Gascon et al. reported the very early study on alkane-selective alkane/alkene separation by a flexible MOF, ZIF-7.<sup>85</sup> ZIF-7 is built on Zn(II) and benzimidazole linkers, with pore aperture of about 3 Å for the activated structure. However, as a result of the structural flexibility, it may accommodate guest molecules larger than 3 Å into

its cages, characterized by the gate-opening step in the adsorption isotherms. Single-component adsorption measurements revealed that the threshold pressure for ethane was much lower than ethylene. As observed for other flexible MOFs, gate-opening pressure relates to the interaction between the adsorbate and the organic linker at the pore window of ZIF-7. The difference in the threshold pressure of ethane and ethylene created a pressure window where ethane is adsorbed while ethylene is not. For the first time, the authors experimentally confirmed that the material was ethane-selective for a binary ethane/ethylene mixture through column breakthrough measurements. It is noteworthy that even though the partial pressure of ethylene in the mixture is higher than its gate-opening pressure in ZIF-7, a remarkable ethane/ethylene selectivity was observed. In a subsequent study,<sup>84</sup> Pires et al. explored the ethane-selective behavior of IRMOF-8. IRMOF-8 is built on Zn(II) and naphthalene-2,6-dicarboxylate and is isoreticular to MOF-5. Single-component adsorption isotherms at 298 K up to 10 bar revealed the material favored ethane over ethylene and was confirmed by column breakthrough experiments using ethylene/ethane binary mixtures as the feed. Density functional theory (DFT) calculations indicated that the contributions from the two adjacent rings in the MOF structure result in a higher interaction energy for ethane than that of ethylene. The authors concluded that MOFs with organic linkers with high aromaticity are prone to be ethane-selective materials.

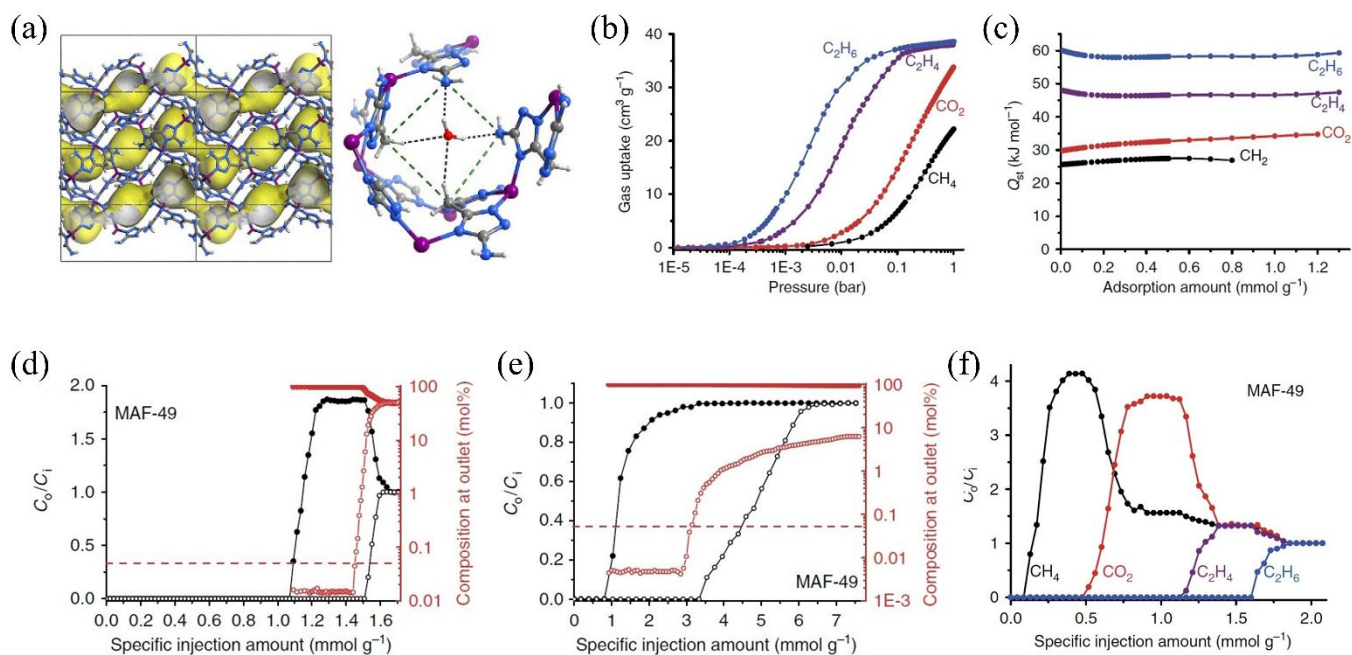


**Figure 6.** a) X-ray crystal structure of MAF-49 · H<sub>2</sub>O. b) Gas adsorption isotherms for C<sub>2</sub>H<sub>6</sub>, C<sub>2</sub>H<sub>4</sub>, CO<sub>2</sub> and CH<sub>4</sub> in MAF-49 at 316 K. c) Coverage-dependent C<sub>2</sub>H<sub>6</sub>, C<sub>2</sub>H<sub>4</sub>, CO<sub>2</sub> and CH<sub>4</sub> adsorption enthalpy obtained by the Virial method. d) C<sub>2</sub>H<sub>4</sub>/C<sub>2</sub>H<sub>6</sub> (1:1) mixture breakthrough curves of MAF-49. e) C<sub>2</sub>H<sub>4</sub>/C<sub>2</sub>H<sub>6</sub> (15:1) mixture breakthrough curves of MAF-49. f) Breakthrough curves of CH<sub>4</sub>/CO<sub>2</sub>/C<sub>2</sub>H<sub>4</sub>/C<sub>2</sub>H<sub>6</sub> mixture (1:1:1:1 (vol)) for MAF-49 measured at 313 K and 1 bar. Reproduced with permission.<sup>83</sup> Copyright 2015, Springer Nature.

An important study in the early explorations for MOFs that preferentially adsorb alkanes over alkenes was carried out by Zhang et al. on MAF-49 (Figure 6).<sup>83</sup> Different from the previously reported alkane-selective MOFs which generally possessed low-polarity or hydrophobic pore surface, MAF-49 featured rather polar pore functionality. The compound was constructed from Zn(II) and bis(5-amino-1H-1,2,4-triazol-3-yl)methane) (H<sub>2</sub>batz) as the organic linker, synthesized solvothermally in aqueous ammonia solution. The ligand was designed to have multiple nitrogen atoms as hydrogen-bonding acceptors and methylene groups as dipole repulsion groups. MAF-49 possesses 1D zigzag channels with the narrowest section of 3.3 × 3.0 Å, and multiple electronegative, uncoordinated nitrogen atoms at pore surface that may be involved in hydrogen bonding. Single-component adsorption isotherms at 316 K revealed ethane is notably favored at low pressure compared to ethylene although the saturation uptake at 1 bar are similar for the two gases. Heats of adsorption calculations indicated the Q<sub>st</sub> for ethane is 60 kJ/mol, higher than that for ethylene (48 kJ/mol). The relatively high adsorption affinity of ethane suggested that multiple supramolecular interactions may exist between ethane and the framework. This was confirmed by GCMC simulation and further periodic DFT optimization of the host-guest structures. Ethane interacted with the pore surface of MAF-49 through multiple strong C-H···N hydrogen bonds and weak electrostatic

interactions while for ethylene the extent of these interactions was much weaker. Feasibility of ethane/ethylene separation by MAF-49 was evaluated by column breakthrough measurements using a binary mixture of 15:1 ethylene/ethane as a feed, mimicking industrial mixtures produced by hydrocarbon cracking. It was revealed that ethylene with a purity of 99.995% can be obtained through a single breakthrough step with an ethylene productivity of 1.68 mmol/g (99.95%+ purity). This was much more efficient than previously reported ethane-selective MOFs such as IR-MOF-8 and MAF-4 under identical conditions. This study indicated that ethane-selective MOFs may be achievable by rational utilization of polar functional groups and optimization of surface electrostatic distribution that may result in stronger binding to ethane over ethylene.

Li et al. demonstrated the exceptional ethane-selective ethane/ethylene separation by Fe<sub>2</sub>(O<sub>2</sub>)dobdc in 2018 (Figure 7).<sup>20</sup> The material, Fe<sub>2</sub>(O<sub>2</sub>)dobdc, was developed by Long et al. early in 2011 through the oxidation of solvent-free Fe<sub>2</sub>(dobdc) by oxygen.<sup>86</sup> Fe<sub>2</sub>(O<sub>2</sub>)dobdc retains the crystal structure of its parent compound Fe<sub>2</sub>(dobdc) upon functionalization, but is characterized by the iron(III)-peroxo sites on its pore surface. In contrast to the pristine MOF Fe<sub>2</sub>(dobdc) which favors ethylene over ethane, Fe<sub>2</sub>(O<sub>2</sub>)dobdc shows notable preference to ethane. It adsorbed 3.3 mmol/g of ethane at 298 K and 1 bar, noticeably higher than that of ethylene (2.5 mmol/g) under identical conditions. Ethane showed a Q<sub>st</sub> of 66.8 kJ/mol, higher than

other ethane-selective MOFs including the previous illustrated MAF-49, indicating the strong interaction between ethane and the framework. The gas-MOF interaction was uncovered by neutron powder diffraction (NPD) measurements. It was revealed that ethane molecules preferentially interacted with the peroxy sites through C-H  $\cdots$ O hydrogen bonds. DFT calculations further confirmed the preferential binding sites suggested by NPD, indicating that the ethane/ethylene adsorption selectivity was a result of the peroxy active sites and the electronegative surface oxygen distribution in  $\text{Fe}_2(\text{O}_2)\text{dobdc}$ . Remarkably,  $\text{Fe}_2(\text{O}_2)\text{dobdc}$  exhibited an ethane/ethylene IAST selectivity of 4.4 at 298 K and 1 bar, outperforming the previously reported ethane-selective MOFs such as MAF-49 and IR-MOF-8. The authors carried out systematic column breakthrough measurements with different

multicomponent feeds, demonstrating the capability of  $\text{Fe}_2(\text{O}_2)\text{dobdc}$  for the separation of ethane and ethylene. It is noteworthy that the authors in this work not only demonstrated a distinct MOF material for highly efficient separation of ethane and ethylene through ethane-selective adsorption, but also developed a general approach for immobilizing strong adsorption sites to produce alkane-selective adsorbents. The material design strategy has been successfully employed in Cr-BTC and Cu-BTC.<sup>69</sup> Both Cr-BTC( $\text{O}_2$ ) and Cu-BTC( $\text{O}_2$ ) showed selective adsorption of ethane over ethylene, while the adsorption preferences were reversed in their parent structures. However, it is noteworthy that the reported MOFs with metal-peroxy sites are sensitive to moisture and all the measurements were performed under inert atmosphere.

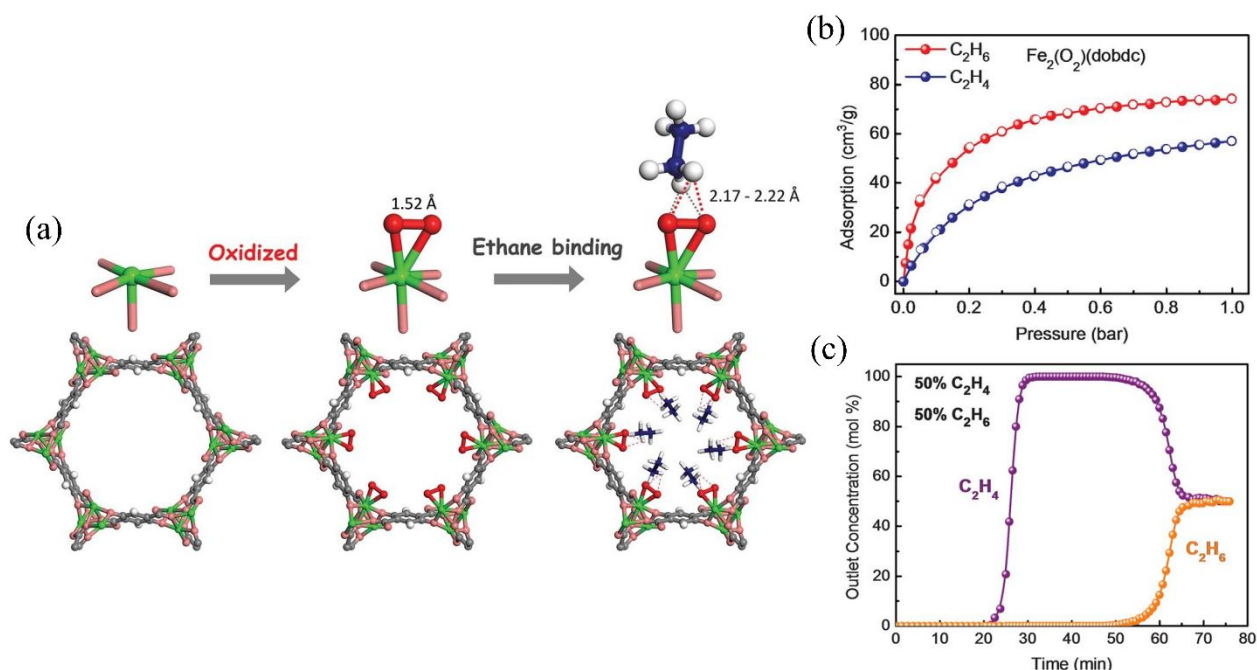


**Figure 7.** a) Structures determined from NPD studies. Shown are structures of  $\text{Fe}_2(\text{dobdc})$ ,  $\text{Fe}_2(\text{O}_2)\text{dobdc}$ , and  $\text{Fe}_2(\text{O}_2)\text{dobdc} \rightarrow \text{C}_2\text{D}_6$  at 7 K. b) Adsorption (solid) and desorption (open) isotherms of  $\text{C}_2\text{H}_6$  (red circles) and  $\text{C}_2\text{H}_4$  (blue circles) in  $\text{Fe}_2(\text{O}_2)\text{dobdc}$  at 298 K. c) Experimental column breakthrough curves for  $\text{C}_2\text{H}_6/\text{C}_2\text{H}_4$  (50/50) mixture in an absorber bed packed with  $\text{Fe}_2(\text{O}_2)\text{dobdc}$  at 298 K and 1.01 bar. Reproduced with permission.<sup>20</sup> Copyright 2018, AAAS.

A surge in the number of reported ethane-selective MOFs since 2018 has been observed. A variety of material design/functionalization strategies have been applied and several studies focusing on computational screening or mechanistic exploration have also been presented. Pinto et al. reported the enhancement of ethane/ethylene adsorption selectivity by the introduction of perfluoro groups in Zr-MOFs.<sup>75</sup> Compared to UiO-66 (Zr-BDC), Zr-NDC, and UiO-66-Br which showed almost identical adsorption toward ethane and

ethylene, UiO-66- $2\text{CF}_3$  exhibited preference for ethane over ethylene. IAST ethane/ethylene adsorption selectivity for UiO-66- $2\text{CF}_3$  was calculated to be 2.5. The selectivity was retained at higher pressures up to 1000 kPa. Computational explorations revealed the possible stronger interaction between the organic linker and ethane than ethylene. This work demonstrated that the introduction bulky  $\text{CF}_3$  groups may be more efficient for the improvement of ethane/ethylene selectivity in MOFs than increasing the aromaticity of the organic linker.

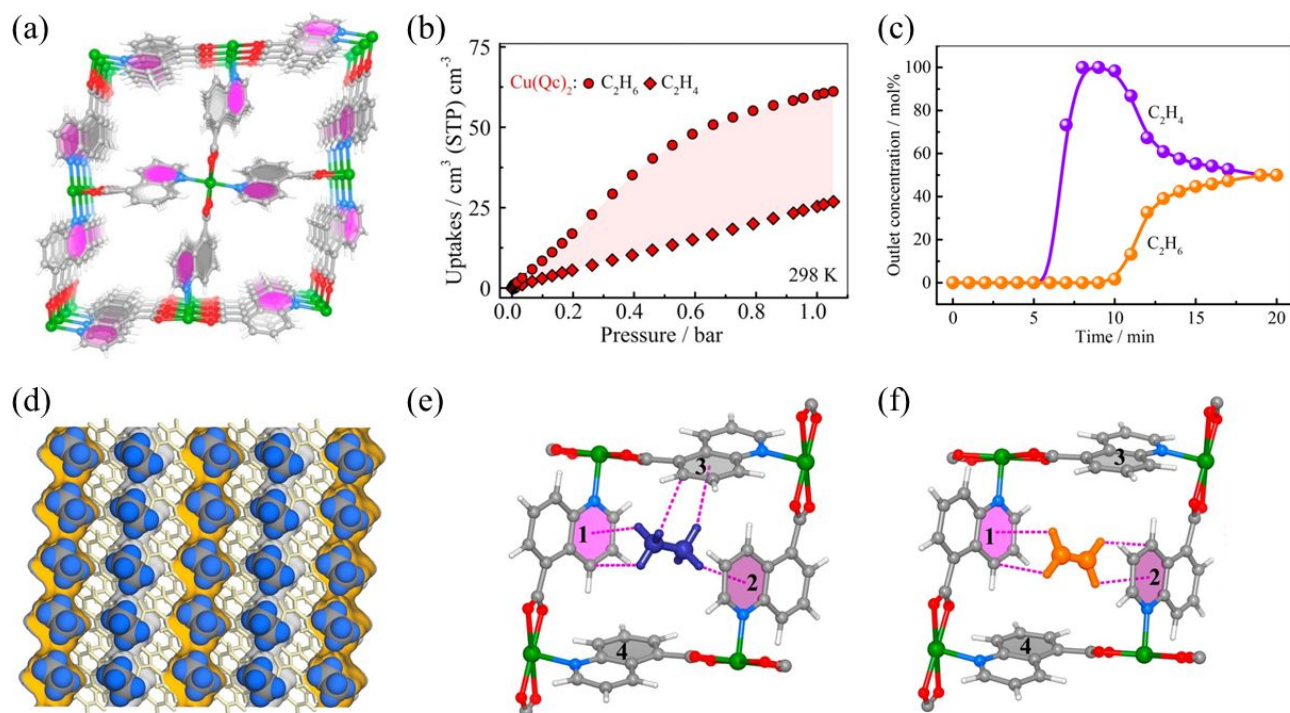


**Figure 8.** a) Crystal structure of Cu(Qc)<sub>2</sub>. b) C<sub>2</sub>H<sub>6</sub> and C<sub>2</sub>H<sub>4</sub> sorption isotherms for Cu(Qc)<sub>2</sub> at 298 K. c) Experimental column breakthrough curves for equimolar C<sub>2</sub>H<sub>6</sub>/C<sub>2</sub>H<sub>4</sub> (orange/purple) mixture (298 K, 1 bar) in an adsorber bed packed with Cu(Qc)<sub>2</sub>. d-e) Neutron diffraction crystal structures of ethane loaded Cu(Qc)<sub>2</sub>. f) Neutron diffraction crystal structures of ethylene loaded Cu(Qc)<sub>2</sub>. Reproduced with permission.<sup>66</sup> Copyright 2018, American Chemical Society.

Chen et al. reported the improvement of ethane/ethylene selectivity by controlling the pore structures in isoreticular, ultramicroporous MOFs.<sup>66</sup> The authors investigated adsorption and separation of ethane and ethylene on Cu(ina)<sub>2</sub> (Hina = isonicotinic acid) and Cu(Qc)<sub>2</sub> (HQc = quinolone-5-carboxylic acid), two microporous structures with the same connectivity but different pore sizes. Cu(Qc)<sub>2</sub> has a pore aperture of 3.3 Å in its activated form, smaller than that of Cu(ina)<sub>2</sub> (4.1 Å). Cu(ina)<sub>2</sub> exhibited slightly higher adsorption capacity for ethane over ethylene. However, ethane-selective adsorption behavior was much more distinct in Cu(Qc)<sub>2</sub> (Figure 8). It adsorbed 1.85 mmol/g of ethane at 298 K and 1 bar, substantially higher than that of ethylene (0.78 mmol/g). IAST ethane/ethylene selectivity was calculated to be 3.4 at 298 K and 1 bar for Cu(Qc)<sub>2</sub>. This value was higher than most of the previously reported ethane-selective adsorbents. Column breakthrough measurements of an equimolar ethane/ethylene mixture revealed that the material was capable of separating ethane and ethylene. The resulting ethylene that eluted was detected to have 99.9%+ purity at the outlet before the breakthrough of ethane. The underlying mechanism of favored adsorption of ethane over ethylene by Cu(Qc)<sub>2</sub> was explored through neutron powder diffraction studies. The results indicated that the cavity of Cu(Qc)<sub>2</sub> was optimal for the accommodation of ethane which enabled the binding for ethane molecules through multiple C-H ... π interactions. In comparison, the resulting interactions

between ethylene molecules and the cavities result in lower binding affinity. The authors concluded that an applicable design strategy to produce ethane-selective MOFs with high efficiency would include increasing the efficient contact area or the number of specific interactions between the pore surface and ethane. More recently,<sup>65</sup> Tang et al. reported the facile synthesis of Cu(Qc)<sub>2</sub> by stirring at room temperature to produce a highly crystalline phase within 1 hour. The material prepared at room temperature (termed as RT-Cu(Qc)<sub>2</sub>) showed higher ethane uptake and lower ethylene uptake at 298 K at 1 bar, resulting in higher ethane/ethylene uptake ratio and selectivity. The IAST ethane/ethylene selectivity for RT-Cu(Qc)<sub>2</sub> was 4.1, outperforming most of the previously reported ethane-selective MOFs. Nevertheless, it was not clear that why the Cu(Qc)<sub>2</sub> synthesized at room temperature performed better than the one prepared from solvothermal reactions.

Feng et al. developed a series of ethane-selective MOFs with high ethane uptake through the pore-space-partition (PSP) strategy.<sup>70</sup> The materials were built on MIL-88 type framework by introducing a pore partitioning agent into its hexagonal channel, with a resultant formula of [(M<sub>1</sub><sub>2</sub>M<sub>2</sub>)(O/OH)L<sub>1</sub>]<sub>3</sub>L<sub>2</sub>, where M<sub>1</sub> and M<sub>2</sub> are the metals in the trimer of the acs net, L<sub>1</sub> is the dicarboxylate ligand for the formation of the pristine framework, and L<sub>2</sub> is the tripyridyl pore-partitioning agent. The pore-partitioning agents not only partitioned the channel into smaller pores, but also deactivated all the open metal sites in

## REVIEW

the original acs framework. This process changed the adsorbents from ethylene-selective to ethane-selective. By experimental exploration of 9 compounds in this family, the authors demonstrated the exceptionally high ethane uptake of these ethane-selective adsorbents. In particular, CPM-233 ( $\text{Mg}_2\text{V-bdc-tpt}$ ) took up  $166 \text{ cm}^3/\text{g}$  ( $7.45 \text{ mmol/g}$ ) of ethane at 298 K and 1 bar, substantially higher than that for PCN-250 ( $117 \text{ cm}^3/\text{g}$ ), the previous benchmark material for ethane uptake among ethane-selective adsorbents. In addition, the  $Q_{\text{st}}$  for ethane in these materials were generally low, in the range of 21.9–30.4 kJ/mol, much lower than those with strong ethane-adsorption sites such as  $\text{Fe}_2(\text{O}_2)(\text{dobdc})$ . The relatively low adsorption heat may be advantageous with respect to energy consumption associated with adsorbent regeneration. The IAST ethane/ethylene selectivities of these materials are between 1.4 to 1.75, comparable to most of the reported ethane-selective MOFs, but are significantly lower than the top-performing ones such as  $\text{Fe}_2(\text{O}_2)(\text{dobdc})$  and  $\text{Cu}(\text{Qc})_2$ . This study provided a valuable approach for achieving high adsorption capacity for ethane-selective MOFs. In a more recent work,<sup>56</sup> the same research group developed a series of MOFs built on 8-connected  $\text{M}_3(\text{OH})(\text{OOCR})_5(\text{Py-R})_3$  trimers ( $\text{M} = \text{Zn}, \text{Co}, \text{Fe}$ ) through the so-called angle bending modulation strategy. Similar to the foregoing materials obtained via PSP approach, these newly-developed MOFs (CPM-80–82) exhibited favored adsorption of ethane over ethylene with high ethane uptake as well. For example, CPM-81-Co adsorbed  $123 \text{ cm}^3/\text{g}$  of ethane at 298 K and 1 bar, with an ethane/ethylene IAST selectivity of 1.8.

The foregoing ethane-selective MOFs generally possess ethane/ethylene IAST selectivities of 1 to 4. In contrast, substantially higher ethane/ethylene selectivities have recently been achieved in a series of mesoporous MOFs (Figure 9), the NIIC-20 family, developed by Fedin et al. They were built on  $\text{Zn}_{12}(\text{RCOO})_{12}(\text{glycol})_6$  rings, featuring 25 Å interconnected cages.<sup>57</sup> The materials were synthesized through solvothermal reactions of zinc nitrate, isophthalic acid, dabco, and the corresponding glycol in DMF. Taking NIIC-20-Bu as an example, it adsorbed 2.5 mmol/g of ethane at 298 K and 1 bar, notably higher than that of ethylene (1.4 mmol/g) under identical conditions, resulting in an ethane/ethylene IAST selectivity of 15.4 for an equimolar ethane/ethylene binary mixture. The selectivity is the new record for all ethane-selective adsorbents. Computational studies revealed that the preferential adsorption of ethane over ethylene in these materials originated from the stronger adsorption affinity of ethane in the nanocages, with the formation of strong C-H...O hydrogen bonds.

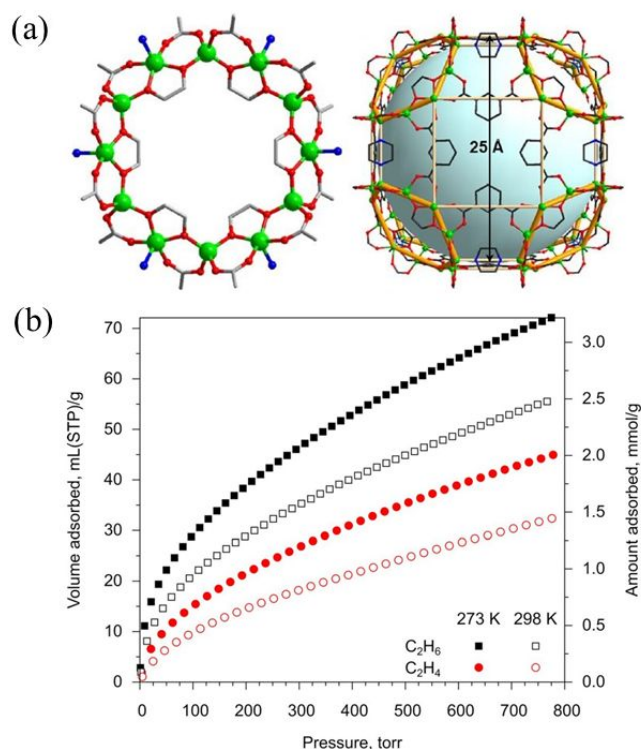


**Figure 9.** a) Crystal structure of NIIC-20-Et. b) The adsorption isotherms of  $\text{C}_2\text{H}_6$  and  $\text{C}_2\text{H}_4$  at 273 K (filled symbols) and 298 K (empty symbols) for NIIC-20-Bu. Reproduced with permission.<sup>57</sup> Copyright 2020, Wiley VCH.

Compared to the rapid development of ethane-selective adsorbents over the past few years, propane-selective adsorbents are much scarcer. A likely factor that may contribute to this is the smaller difference in molecular size and physical properties between propane and propylene, compared to that of ethane and ethylene. Xing et al. reported propane-selective propane/propylene separation by an anion-pillared microporous MOF,  $\text{Ni}(\text{bpe})_2(\text{WO}_4)$  (WOFour-1-Ni).<sup>45</sup> Interestingly, the material adsorbed more propylene than propane at 298 K and 1 bar, but propane was favored at low pressure. The heat of adsorption for propane was also slightly higher than that of propylene. The calculated propane/propylene IAST selectivity was 1.6. Its propane-selective behavior was confirmed in the multicomponent column breakthrough measurements where propylene broke prior to propane. GCMC simulation and DFT calculations revealed that the preferential adsorption of propane over propylene originated from stronger adsorption affinity of propane in the polycatenated molecular cages along with a certain degree of shape selectivity. More recently, Li et al. reported propane-selective adsorption by a modified UiO-type MOF, BUT-10.<sup>46</sup> Similar to that of the foregoing WOFour-1-Ni, BUT-10 also showed propane-favored adsorption at relatively low pressure region, with higher adsorption affinity than that of propylene. It exhibited an IAST selectivity of 1.4, slightly lower

than that of WOFUR-1-Ni, but a much higher adsorption capacity for propane (105 cm<sup>3</sup>/g) at 298 K and 1 bar.

Besides the foregoing experimental explorations for alkane-selective MOFs, computational studies exploiting the underlying adsorption mechanisms and design strategies have also been carried out by several research groups. Siperstein et al. applied GCMC simulations to investigate the influence of pore size and pore shape on ethane/ethylene selectivity in ethane-selective adsorbents.<sup>87</sup> They used a model by adding 4,4'-bipyridine pillars in slit pores to mimic MOF structures. With this simulation model, the authors successfully predicted the selectivity for many of the ethane-selective adsorbents. In particular, the authors concluded that ethane/ethylene adsorption selectivity based on van der Waals interactions cannot be higher than 2.8. However, higher selectivities toward ethane may be achieved if the MOF pores have strong electric field gradients that prevent the adsorption of ethylene or the pores are very small and fit better with ethane molecules. In another study, Jiang et al. performed computational screening study on a large set (1747) of MOFs structures and established quantitative relationships between adsorption performance (ethane/ethylene selectivity and capacity) and the structural descriptors (pore size, surface area etc.).<sup>88</sup> The results indicated that the ethane/ethylene separation performance of a MOF is a complex interplay of the structural descriptors. Based on the computational findings, the authors proposed six design strategies for developing ethane-selective MOFs with high performance: regulating topology, catenating framework, adding aromatic ring, pillar-layering framework, substituting metal node, and imposing flexibility.

Covalent organic frameworks (COFs) and hydrogen-bonded organic frameworks (HOFs) have also been explored for selective capture of ethane from ethane/ethylene mixtures. Li et al. reported the systematic regulation of pore channels in COFs for selective removal of ethane from ethylene.<sup>89</sup> Eight representative COFs with

various pore sizes and pore environments, including COF-1, COF-6, COF-8, COF-10, MCOF-1, COF-102, COF-300, and COF-320, were selected for the evaluation of their adsorption and separation of ethane and ethylene. Several of them show notable preference to ethane over ethylene, which was attributed to a large quantity of nonpolar benzene rings leading to strong C-H... $\pi$  interactions with ethane. COF-1 was identified as the optimal adsorbent with an ethane/ethylene selectivity of 1.92 at 298 K and 1 bar, as a result of its richly distributed weakly polar surface and suitable pore dimensions. Chen et al. reported a series of microporous HOFs using hexacarboxylate ligands as building blocks.<sup>90, 91</sup> These HOFs feature permanent porosity, good thermal stability, and high water resistance. Particularly, due to the nonpolar pore surfaces in these materials, they exhibit ethane-favored adsorption over ethylene with an ethane/ethylene selectivity of 2-3.

### 3. Kinetic separation

Compared to the foregoing thermodynamic separation, kinetic separation of alkane/alkene is relatively rare as it has stringent requirements on the pore size of MOFs. Early in 2009, Li et al. reported the kinetic separation of propane and propylene by ZIF-8 and its isoreticular Zn(2-cim)<sub>2</sub>.<sup>92</sup> While propane and propylene showed essentially identical adsorption capacity on these materials, they exhibited distinct adsorption kinetics. At 30 °C, the ratios of the diffusion rate coefficients, D(propane)/D(propylene), were 125 and 60 for ZIF-8 and Zn(2-cim)<sub>2</sub>, respectively. Obviously, the separation of propane and propylene by ZIF-8 and Zn(2-cim)<sub>2</sub> was controlled by the critically sized pore openings. It was measured from the crystal structures that the pore apertures are 3.26 and 3.37 Å for ZIF-8 and Zn(2-cim)<sub>2</sub>, respectively.

Table 2. Representative MOFs showing kinetic separation for alkane/alkene

MOF	BET surface area (m <sup>2</sup> /g)	Aperture size (Å)	Uptake (mmol/g)		Selec.	Temp. (K)	Ref.	
			alkene	alkane				
ZIF-8	/	3.3	/	/	125	303	92	
Zn(2-cim) <sub>2</sub>	/	3.4	/	/	60	303	92	
DTO	669	5.3	/	/	1.4	298	93	
TO	512	5.4	/	/	2.5	298	93	
DBTO	457	5.1	/	/	11	298	93	
BTO	283	4.7	/	/	12	298	93	
C <sub>3</sub> H <sub>8</sub> /C <sub>3</sub> H <sub>6</sub>	Zn(ox) <sub>0.5</sub> (trz)	546	2.9	2.3	/	860	303	94
	Zn(ox) <sub>0.5</sub> (atrz)	521	2.6	1.7	/	175	303	94
	ftw-MOF-ABTC	/	4.4	2.3	2.5	/	298	95
	ELM-12	/	4.0	1.5	1.4	204	298	96
	MAF-23-O	/	3.6	1.4	1.2	71	298	97
	Co <sub>2</sub> (5-aip) <sub>2</sub> (bpy)	/	/	2.0	0.5	21	298	98
	ZnAtzPO <sub>4</sub>	420	3.8	1.1	0.3	31	298	99
C <sub>2</sub> H <sub>6</sub> /C <sub>2</sub> H <sub>4</sub>	GT-18	/	3	0.6	0.2	6.8	298	100
	Cu(OPTz)	/	/	2.3	0.4	6	300	101
	ZnAtzPO <sub>4</sub>	/	4.9	1.9	1.0	12	298	102

Notes: (1) Gas uptakes were measured at the specified temperature and 1 bar. (2) Selectivities were calculated by the IAST model.

In a subsequent study, Nguyen et al. carried out a systematic investigation on kinetic separation of propane and propylene in a series of isorecticular MOFs by tuning their pore apertures and crystallite aspect ratios.<sup>93</sup> These pillared paddlewheel MOFs built from 1,2,4,5-tetrakis(carboxyphenyl)benzene and trans-1,2-dipyridylethene linkers were synthesized solvothermally in DMF with the addition of aqueous hydrogen chloride. With a series of four isostructural MOFs, DTO, TO, DBTO, BTO, with decreasing aperture size from 5.27 to 4.67 Å, they showed increasing propylene/propane kinetic selectivity from 1.4 to 12. Interestingly, the authors attempted to optimize propylene/propane selectivity through tuning of the pore apertures (via -Br functionalization) and modulation of channel congestion (via the introduction of TMS group). The results indicated that the former strategy exhibited noticeably more appreciable effects on the propylene/propane kinetic selectivity. In addition, investigation of the influence of crystallite aspect ratios revealed that the orientation of the channel perpendicular to the largest faces of the crystals was necessary for achieving high kinetic selectivity. Li et al. explored the kinetic separation of propylene and propane on two ultramicroporous MOFs, Zn(ox)<sub>0.5</sub>(trz) and Zn(ox)<sub>0.5</sub>(atrz) (ox = oxalate, trz = 1,2,4-triazole, atrz = 3-amino-1,2,4-triazole).<sup>94</sup> These two compounds feature 1D zigzag channels with narrow necks of 2.9 and 2.6 Å for Zn(ox)<sub>0.5</sub>(trz) and Zn(ox)<sub>0.5</sub>(atrz),

respectively. Both materials exhibited marked diffusional restrictions. Propylene/propane kinetic selectivity for Zn(ox)<sub>0.5</sub>(trz) reached 1565 at 323 K while for Zn(ox)<sub>0.5</sub>(atrz) the selectivity was 220. These values were substantially higher than that of the previously reported ZIF-8 and TO series. The high selectivities were attributed primarily to the appropriate pore apertures. Li et al. reported the kinetic separation of propylene and propane by ELM-12 (Cu(bipy)<sub>2</sub>(OTf)<sub>2</sub>, bipy = 4,4'-bipyridine, OTf = triuoromethanesulfonate).<sup>96</sup> ELM-12 possesses zigzag 2D channels with pore window of around 4.0 Å, and features high stability and facile scale-up preparation. The adsorption of propylene on ELM-12 showed no diffusional restrictions and reached equilibrium within 1-2 minutes. In contrast, severe diffusion limitations were observed for propane, resulting in propylene/propane kinetic selectivities of 204 and 971 at 298 and 308 K, respectively, comparable to that of Zn(ox)<sub>0.5</sub>(trz) and Zn(ox)<sub>0.5</sub>(atrz). Separation capability of ELM-12 was experimentally confirmed by column breakthrough measurements, which exhibited a clear separation for an equimolar propylene/propane binary mixture. Highly selective alkane/alkene separation may be achieved by tailoring pore size or pore environment of MOFs, or by post-synthetic modification of their pore functionality. This was nicely demonstrated in the case of Fe<sub>2</sub>(O<sub>2</sub>)dobdc.

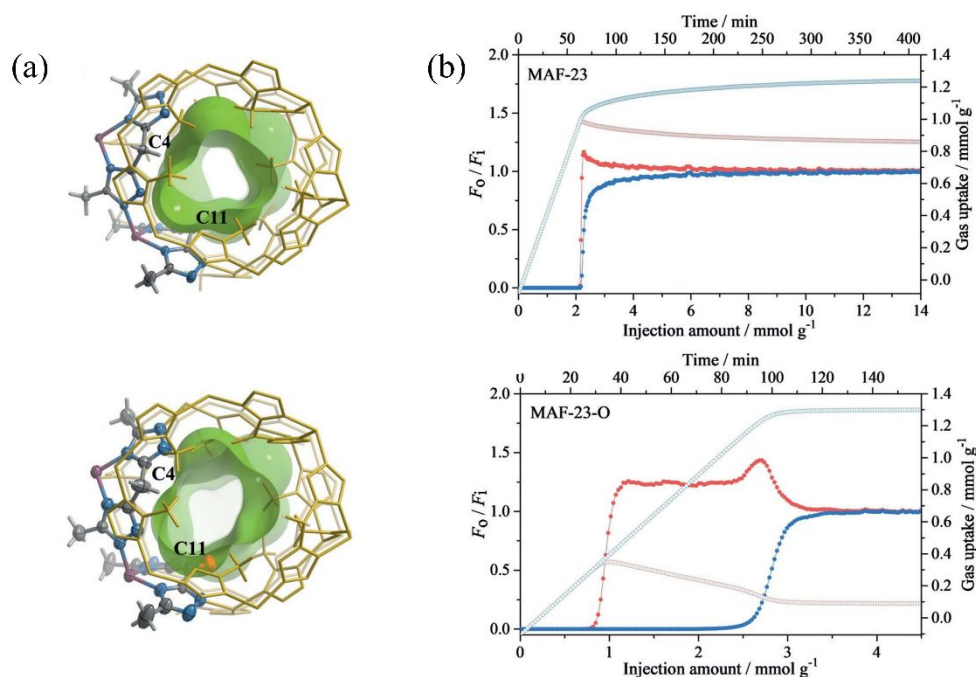


**Figure 10.** a) Crystal and pore structures of (Top) MAF-23 and (Top) MAF-23-O. The asymmetric units are drawn with thermal ellipsoids (50% probability). The two independent methylene/carbonyl groups are highlighted by atom labeling. b) Breakthrough curves (solid) and adsorption kinetic curves (open) for (Top) MAF-23 and (Bottom) MAF-23-O using an equimolar C<sub>3</sub>H<sub>6</sub>/C<sub>3</sub>H<sub>8</sub> (blue/red) mixture (1 cm<sup>3</sup>min<sup>-1</sup>) at 298 K and 1 atm. Lines are drawn to guide the eye. F<sub>i</sub> and F<sub>o</sub> are the flow rates of each gas at

the inlet and outlet, respectively. The negative gas uptakes shown in the initial regions are equal to the gas amount in the dead space of the breakthrough manifold. Reproduced with permission.<sup>97</sup> Copyright 2019, VCH.

More recently, Zhang et al. reported the post-synthetic functionalization of MAF-23 to MAF-23-O and its kinetic separation of propane and propylene. MAF-23 is built on Zn(II) and  $\text{btm}^{2-}$  ( $\text{H}_2\text{btm} = \text{bis}(5\text{-methyl-1H-1,2,4-triazol-3-yl)methane}$ ).<sup>97</sup> It showed no noticeable thermodynamic or kinetic separation toward propane and propylene (Figure 10). Upon oxidation of MAF-23,  $\text{btm}^{2-}$  was converted to  $\text{btk}^{2-}$  ( $\text{H}_2\text{btk} = \text{bis}(5\text{-methyl-1,2,4-triazol-3-yl)methanone}$ ), leading to the formation of MAF-23-O which retained the structure of MAF-23. The reaction was carried out by heating the pristine MAF-23 at 140 °C in oxygen for 1500 minutes. The conversion ratio of the oxidation reaction was 50%, meaning both  $\text{btm}^{2-}$  and  $\text{btk}^{2-}$  were present in the newly formed compound. This subtle change in the organic linker dramatically affected the pore size and pore environment of the MOF, and thus noticeably improved its propane/propylene separation performance. The propylene/propane kinetic selectivity was calculated to be 112.3 for MAF-23-O, two orders of magnitude higher than that of its parent structure. Interestingly, thermodynamic selectivity of propylene/propane was also enhanced as a result of the formation of the carbonyl bridges in the structure. The separation capability of MAF-23-O was confirmed by experimental column breakthrough measurements which yielded a propylene/propane selectivity of 15. This study demonstrated the subtle structural change through post-synthetic modification may have dramatic effect on kinetic and/or thermodynamic separation of alkane/alkene mixtures.

Kinetic separation of ethylene and ethane has been relatively rarely reported compared to that for propylene and propane. In a recent study, Lively et al. explored kinetically-controlled

separation of ethylene and ethane by a mixed-linker MOF, GT-18.<sup>100</sup> GT-18 was constructed on Zn(II) and two organic linkers benzotriazole (BTA) and benzimidazole (BIM) with a molar ratio of 4:1. It features a similar structure to that of ZIF-7, with an aperture size of  $\sim 3$  Å. While simulated adsorption isotherms for ethylene and ethane were almost identical, experimental isotherms under pseudo-equilibrium indicated ethylene was noticeably favoured. Measurements of adsorption kinetics revealed the diffusion of ethane was largely restricted compared to ethylene, leading to an ethylene/ethane kinetic selectivity of 6.8. This study demonstrates a simple strategy for fine-tuning MOF pore apertures for alkane/alkene kinetic separation by employing mixed linkers with suitable dimensions.

Kitagawa et al. explored the adsorption of ethylene and ethane on a flexible porous coordination polymer, Cu(OPTz) (OPTz = phenothiazine-5,5-dioxide).<sup>101</sup> The compound features flexible structure with flip-flop molecular motions within the framework that function as a gate for guest encapsulation and exclusion. Gas adsorption on Cu(OPTz) was highly temperature-dependent. Measurements of isobar revealed that the adsorption capacity of ethylene increased as a function of increasing temperature and reached maximum capacity at 310 K, after which the adsorbed amount decreased with further increases in temperature. In contrast, the adsorption of ethane increased gradually as temperature increased and the adsorption capacity was noticeably lower than that for ethylene. Ethylene/ethane selectivity was calculated to be  $\sim 75$  for Cu(OPTz). This study demonstrated making use of the temperature-dependent gating effect for the kinetic separation of ethane and ethylene.

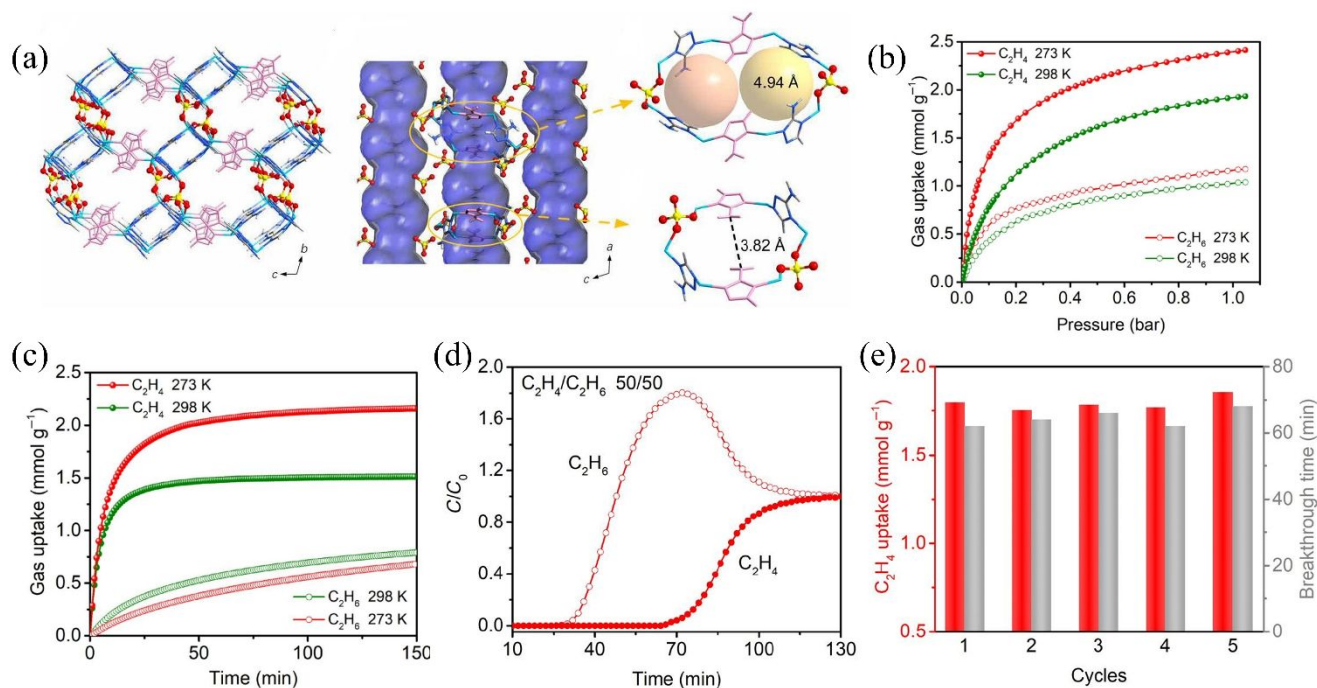


**Figure 11.** a) Schematic illustration of the structure of ZnAtzPO<sub>4</sub>. b) Single-component adsorption isotherms of C<sub>2</sub>H<sub>4</sub> and C<sub>2</sub>H<sub>6</sub> on ZnAtzPO<sub>4</sub> under 298 and 273 K. c) Time-dependent gas uptake profiles of C<sub>2</sub>H<sub>4</sub> and C<sub>2</sub>H<sub>6</sub> at 0.4 bar and different temperatures. d) Breakthrough curve of ZnAtzPO<sub>4</sub> for C<sub>2</sub>H<sub>4</sub>/C<sub>2</sub>H<sub>6</sub> gas mixture (50:50, v/v) at 273 K and 1 bar with a flow rate of 0.75 ml/min. e) Recycling breakthrough tests for C<sub>2</sub>H<sub>4</sub>/C<sub>2</sub>H<sub>6</sub> (50:50, v/v) separation with ZnAtzPO<sub>4</sub>. Reproduced with permission.<sup>102</sup> Copyright 2020, AAAS.

Many of the foregoing separations result from a combined effect of thermodynamic separation and kinetic separation, but one dominates the other. However, in certain cases, both thermodynamic and kinetic mechanisms are main contributors and show a markedly synergistic effect on alkane/alkene separation. Xia et al. reported the separation of propane and propylene by a pillar-layer MOF, Zn<sub>2</sub>(aip)<sub>2</sub>(bpy) (aip = 5-aminoisophthalate, bpy = 4,4'-bipyridine).<sup>42</sup> The compound possesses 1D open channels and open metal sites upon removal of free and coordinated solvents. It adsorbed 1.99 mmol/g of propylene at 298 K and 1 bar, substantially higher than that for propane (0.48 mmol/g) under identical conditions. The calculated  $Q_{st}$  for propylene and propane were 42.4 and 33.7 kJ/mol, respectively, indicating higher interaction between the former and the framework. This resulted in a propylene/propane IAST selectivity of 19.8 for an equimolar binary mixture at 100 kPa. Experimental breakthrough measurements confirmed that the material was capable of separating propane and propylene with excellent recyclability. The authors concluded that the separation was based on equilibrium mechanism, however, it is probably a combined effect of thermodynamic and kinetic mechanism. This was confirmed in a subsequent study by the same group, where its analogue compound Co<sub>2</sub>(aip)<sub>2</sub>(bpy) was studied for the adsorption and separation of propane and propylene.<sup>98</sup>

Co<sub>2</sub>(aip)<sub>2</sub>(bpy) exhibited similar separation performance for propane and propylene to its Zn-based analogue, with a IAST selectivity of 21. In this more recent work, the authors carried out additional computational simulations on the adsorption and separation mechanism, and observed the steric hindrance of propane and its low diffusion rate. This was further confirmed by kinetic adsorption experiments which yielded a propylene/propane kinetic selectivity of 29.7.

Xing et al. reported the equilibrium-kinetic synergetic effect for separation of ethylene and ethane by a microporous MOF, ZnAtzPO<sub>4</sub> (Atz = 3-amino-1,2,4-triazole) (Figure 11).<sup>102</sup> ZnAtzPO<sub>4</sub> was prepared solvothermally with 3Zn(OH)<sub>2</sub>·2ZnCO<sub>3</sub>, Atz, and phosphoric acid in a mixed solvent of water and ethanol. The compound is built on 2D ZnAtz cationic layers pillared by PO<sub>4</sub><sup>3-</sup> anions forming a 3D porous framework. The material possesses 1D channels with narrow necks (3.82 Å) and wider chambers (4.94 Å) with the channels decorated by electronegative amino groups from Atz ligands and oxygen atoms from PO<sub>4</sub><sup>3-</sup> anions. Adsorption isotherms at 298 K revealed its ethylene uptake was 1.92 mmol/g at 1 bar, notably higher than that for ethane (1.01 mmol/g) under identical conditions. Kinetic studies indicated the adsorption of ethylene reached equilibrium within about 40 minutes at 298 K, substantially faster than that for ethane which did not reach equilibrium after 150 minutes. The difference in adsorption rates yielded an ethylene/ethane kinetic selectivity

of 36.6 at 298 K. The authors further calculated the equilibrium-kinetic combined selectivity based on their diffusivities and Henry's constants. ZnAtzPO<sub>4</sub> exhibited a combined selectivity of 12.4 at 298 K, higher than those of other kinetically selective adsorbents such as ITQ-55 and Si-CHA under identical conditions. DFT calculations revealed that there were two primary adsorption sites for ethylene molecules where they interact with the pores through multiple hydrogen bonding. In contrast, the adsorption of ethane in the pore induced notable steric hindrance. It is noteworthy that the  $Q_{st}$  for ethylene on ZnAtzPO<sub>4</sub> was 17.3, substantially lower than other adsorbents with or without OMSs. This may be beneficial for material regeneration and was confirmed by column breakthrough

measurements. The material showed excellent recyclability under ambient regeneration through purging with inert gas. In a more recent report,<sup>99</sup> the same research group demonstrated that ZnAtzPO<sub>4</sub> showed similar equilibrium-kinetic separation for propane and propylene. In contrast to ethylene which reached adsorption equilibrium within 40 minutes, the adsorption of propylene was not reaching equilibrium after 180 minutes. And the adsorption of propane was even slower. This resulted in a propylene/propane kinetic selectivity of 11 and an equilibrium-kinetic combined selectivity of 8.5 at 298 K. Similarly, the material featured relatively low heats of adsorption for propylene (27.5 kJ/mol) leading to the mild regeneration condition under column separation.

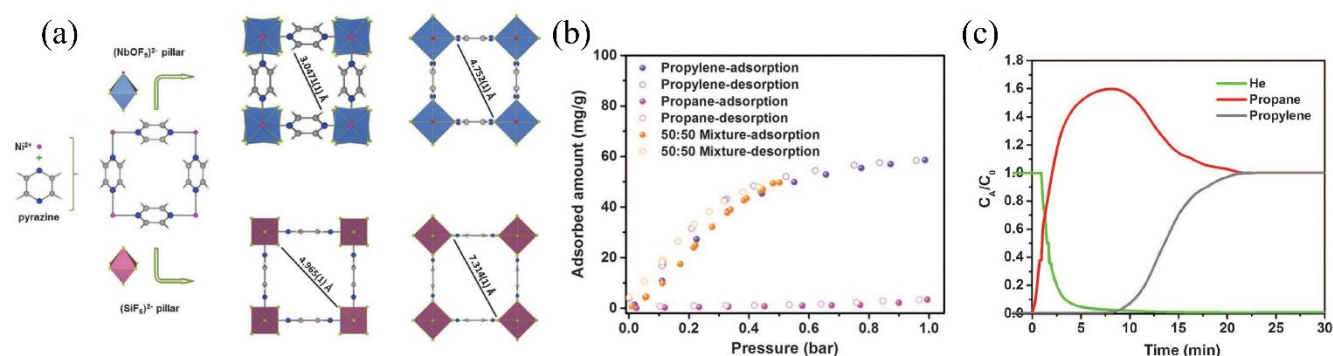


**Figure 12.** a) Structure description of NbOFFIVE-1-Ni (KAUST-7) highlighting the building blocks arrangement and its comparison with the parent SIFSIX-3-Ni. b) The pure C<sub>3</sub>H<sub>8</sub> (pink), pure C<sub>3</sub>H<sub>6</sub> (purple), and equimolar mixture of C<sub>3</sub>H<sub>6</sub>/C<sub>3</sub>H<sub>8</sub> 50/50 (orange) isotherms of NbOFFIVE-1-Ni have been collected at 298 K, demonstrating the full propylene from propane sieving ability of this adsorbent at 1 bar. c) C<sub>3</sub>H<sub>6</sub>/C<sub>3</sub>H<sub>8</sub> 50/50 mixed-gas experiment using a packed column bed at 298 K and a 1 bar total pressure and 4 cm<sup>3</sup>/min total flow, confirming the infinite C<sub>3</sub>H<sub>6</sub>/C<sub>3</sub>H<sub>8</sub> separation factor. Reproduced with permission.<sup>13</sup> Copyright 2016, AAAS.

#### 4. Selective size exclusion

Separation based on selective size exclusion occurs as a special scenario of kinetic separation, where the pore size of the adsorbent is optimal leading to one or more adsorbates being adsorbed while the others being completely excluded. It is considered the ideal separation as it offers the highest possible adsorption selectivity. However, separation through selective size exclusion has stringent requirement on pore size, especially for the alkane/alkene separation where the differences in molecular dimensions are minor. Compared to traditional adsorbent materials, MOFs hold particular promise for selective size exclusion due to its diverse structure and highly tunable pore size. Over the past few years, several MOFs showing selective size-exclusion for alkane/alkene separation have been developed.

KAUST-7 (also denoted as NbOFFIVE-1-Ni) developed by Eddaoudi et al. is the first MOF showing complete sieving of alkane/alkene.<sup>13</sup> It adsorbs propylene but fully excludes propane. It is worth mentioning that the material was rationally designed through reticular chemistry approach. The structure of KAUST-7 is built on Ni(II)-pyrazine square-grid layers pillared

by NbOF<sub>5</sub><sup>2-</sup> struts. The material was prepared hydrothermally with Ni(NO<sub>3</sub>)<sub>2</sub>·6H<sub>2</sub>O and Nb<sub>2</sub>O<sub>5</sub> with the addition of HF. It is a derivative compound of the previously developed SIFSIX-3-Ni with SiF<sub>6</sub><sup>2-</sup> substituted by NbOF<sub>5</sub><sup>2-</sup> aiming at downsizing the pore aperture. The resultant KAUST-7 obtained through topology-directed structure tuning retains the primitive cubic topology with reduced pore aperture of 3.0 to 4.8 Å, depending on the rotation of the NbOF<sub>5</sub><sup>2-</sup> pillars. At 298 K and 1 bar, KASUT-7 adsorbs 60 mg/g of propylene, but shows essentially no adsorption of propane under the identical conditions. This should be attributed to its optimal pore dimensions. The selective molecular exclusion behavior was confirmed by simultaneous calorimetric and gravimetric measurements which shows a heat of adsorption of 57.4 kJ/mol for propylene while no detectable heat change was observed for propane. Multicomponent column breakthrough measurements indicated that KASUT-7 is capable of fully separating propane and propylene. Propane broke out at the outlet immediately without any retention, which confirmed that it was fully excluded by the adsorbent. In contrast, propylene was retained in the column for 8 minutes, equivalent to a dynamic adsorption capacity of 0.6 mmol/g. To evaluate the separation capability of KAUST-7 relating to industrial conditions, the authors applied a

concentration swing recycling mode (CSR) over multiple adsorption-desorption cycles, resulting in a propylene recovery of 2 mol/kg per hour. KAUST-7 outperformed zeolite 4A and 5A under identical conditions. In this work the authors

demonstrated the power of reticular chemistry in fine-tuning pore dimensions of MOFs for challenging size-sieving separations.

Table 3. Representative MOFs showing selective molecular exclusion for alkane/alkene

	MOF	BET surface area (m <sup>2</sup> /g)	Aperture size (Å)	Uptake (mmol/g)		Temp. (K)	Ref.
				alkene	alkane		
C <sub>3</sub> H <sub>8</sub> /C <sub>3</sub> H <sub>6</sub>	KAUST-7	280	4.7	1.4	< 0.1	298	13
	Y-abtc	427	4.7	2.0	< 0.1	298	103
	Co-gallate	486	5.2	1.8	< 0.1	298	104
C <sub>2</sub> H <sub>6</sub> /C <sub>2</sub> H <sub>4</sub>	Co-gallate	475	5.0	5.2	0.3	298	105
	Mg-gallate	559	4.8	4.3	0.3	298	105
	Ni-gallate	424	4.8	3.1	0.3	298	105
	UTSA-280	331	3.8	2.5	< 0.1	298	21

Notes: (1) Gas uptakes were measured at the specified temperature and 1 bar. (2) Selectivities were calculated through the IAST model.

In a subsequent study,<sup>103</sup> Li et al. reported the separation of propane and propylene through selective size exclusion by Y-abtc (Y<sub>6</sub>(OH)<sub>8</sub>(abtc)<sub>3</sub>(H<sub>2</sub>O)<sub>6</sub>(DMA)<sub>2</sub>) (abtc<sup>4-</sup> = 3,3',5,5'-azobenzene-tetracarboxylates; DMA = dimethylammonium). The compound was tailor-made through topology-directed pore size tuning of ftw-type structure based on hexanuclear Zr(IV) or Y(III) clusters. In this work the authors demonstrated the important role of charge balancing cations dimethylammonium (DMA) in Y-MOFs as a regulatory factor to fine tune and control pore dimensions. With a tetratopic ligand, Y-ftw-MOF and Zr-ftw-MOF feature similar connectivity with the former resulting in an anionic framework and the latter a cationic one. Thus the pore size of Y-ftw-MOF is smaller than that of the Zr analogue due to the existence of charge balancing cation. For the same ligand abtc<sup>4-</sup>, Zr-abtc adsorbed both propane and propylene, with similar adsorption capacity and kinetics, showing no separation. In contrast, Y-abtc adsorbed propylene only and fully excluded propane, exhibiting selective molecular exclusion behavior. This should be attributed to its optimal pore size for 4.72 Å. Investigation of adsorption kinetics revealed that it is a case of selective size sieving rather than kinetic separation. Multicomponent column breakthrough measurements confirmed that Y-abtc is capable of full separation of propane and propylene and produces highly pure propylene (99.5+%) that meets the requirements for polymer production. Interestingly, the authors revealed the pore size regulation mechanism by the DMA cations. With relatively low activation temperature, the DMA cations retained intact and the pore size of the MOF is relatively small. However, with increased activation temperature, its pore size increased as DMA cations were converted to protons. This was experimentally confirmed by NMR and gas adsorption studies. The material design strategy in this work may be useful in future

development of ideal adsorbent for efficient alkane/alkene separation.

Bao et al. reported the separation of ethane and ethylene through selective molecular sieving by gallate-based MOFs, Ni/Mg/Co-gallate.<sup>105</sup> These MOFs feature 3D interconnected zigzag channels with pore dimensions of 3.47 × 4.85, 3.56 × 4.84, 3.69 × 4.95 Å<sup>2</sup> for Ni, Mg, Co-gallate, respectively, which are slightly larger than the minimum cross-section size of ethylene. As expected, these compounds adsorbed substantial amount of ethylene but negligible ethane under identical conditions. Taking Co-gallate as an example, its uptake of ethylene is 3.37 mmol/g at 298 K and 1 bar, notably higher than that of ethane (0.31 mmol/g). Multicomponent column breakthrough measurements confirmed that ethane and ethylene can be fully separated by these materials. Interestingly, more recently, Chen et al. reported the full separation of propane and propylene, using the same material Co-gallate.<sup>104</sup> It adsorbed 66.6 cm<sup>3</sup>/cm<sup>3</sup> of propylene at 298 K and 1 bar, while its uptake for propane was negligible (< 6 cm<sup>3</sup>/cm<sup>3</sup>), suggesting its selective molecular sieving behavior. With respect to volumetric adsorption capacity of propylene, Co-gallate outperforms KAUST-7 and Y-abtc, the other two MOFs showing selective molecular sieving for propane and propylene, although its gravimetric uptake is lower. Its separation capability was confirmed by column breakthrough measurements which showed complete separation of the two gases. With an equimolar binary mixture as a feed, propylene with a purity of 97.7% was produced through a single PSA process. These two studies suggest that with optimal pore shape and pore size, one adsorbent may be capable of separating both propane/propylene and ethane/ethylene through selective size sieving.

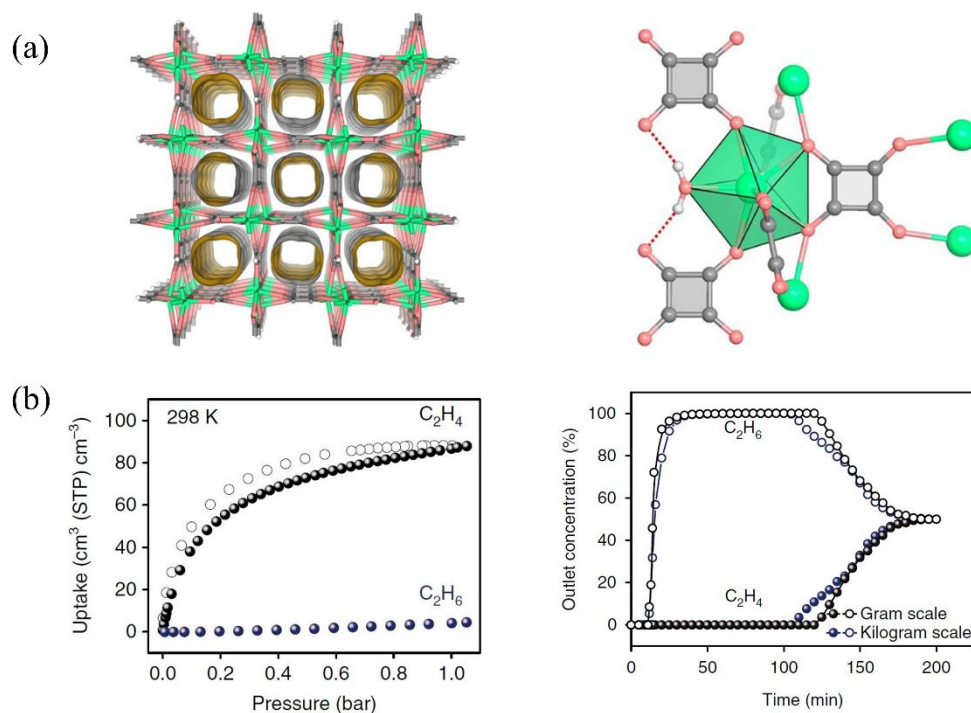


**Figure 13.** a) The crystal structure of guest-free UTSA-280 determined from single-crystal X-ray diffraction, showing one-dimensional channels viewed along the [001] direction. Green, light coral and grey nodes represent Ca, O and C atoms, respectively and the local coordination environments of the squarate linker and calcium atoms. b) (left) Single-component sorption isotherms of ethylene (black) and ethane (blue) at 298 K and (right) Breakthrough curves for UTSA-280 from different scales for an equimolar binary mixture of C<sub>2</sub>H<sub>4</sub>/C<sub>2</sub>H<sub>6</sub> at 298 K and 1 bar. The breakthrough experiments were carried out in a packed column with 3.2 g sample at a flow rate of 2 ml • min<sup>-1</sup>. The points are experimental data, and the lines are drawn to guide the eye. Reproduced with permission.<sup>21</sup> Copyright 2018, Springer Nature.

Another important work in adsorptive separation of ethylene and ethane by MOFs was reported by Chen et al. in 2018,<sup>21</sup> where selective molecular exclusion was achieved by Ca(C<sub>4</sub>O<sub>4</sub>)(H<sub>2</sub>O) (or UTSA-280, H<sub>2</sub>C<sub>4</sub>O<sub>4</sub> = squaric acid). The compound was originally reported in 1987,<sup>106</sup> featuring a 3D framework with 1D channels. The material features facile synthesis, and can be prepared at large scale at room temperature by mixing a saturated aqueous solution of sodium squarate with an aqueous solution of calcium nitrate. The cross-sectional area of the channels is 14.4 Å<sup>2</sup>, falling between the minimum cross-sectional areas of ethylene (13.7 Å<sup>2</sup>) and ethane (15.5 Å<sup>2</sup>), indicating its potential for the separation of the two gases. Indeed, experimental gas adsorption measurements confirmed UTSA-280 was capable of splitting ethane and ethylene. It adsorbed 2.5 mmol/g of ethylene at 298 K and 1 bar while ethane was essentially excluded by the material (uptake < 0.1 mmol/g) under identical conditions. The matching between the size/shape of ethylene and the channel dimensions led to its relatively high adsorption capacity. This was confirmed by gas-loaded single-crystal X-ray diffraction and computational modeling. Crystal structure of ethylene-loaded UTSA-280 revealed that ethylene molecules adopted optimal orientation, with its minimum cross-section along the diagonal of the pore aperture to minimize any possible steric hindrance

and electrostatic repulsion from the framework. In contrast, significant steric hindrance will be unavoidable when ethane molecules are put inside the channels with random orientations, in good agreement with the noticeably higher potential energy variations for ethane along the channels from DFT calculations. Ethane/ethylene separation ability of UTSA-280 was confirmed by column breakthrough measurements with binary ethane/ethylene and octonary H<sub>2</sub>/CH<sub>4</sub>/C<sub>2</sub>H<sub>2</sub>/C<sub>2</sub>H<sub>4</sub>/C<sub>2</sub>H<sub>6</sub>/C<sub>3</sub>H<sub>6</sub>/C<sub>3</sub>H<sub>8</sub>/C<sub>4</sub>H<sub>8</sub> mixtures. The results indicated that the adsorbent was capable of enriching ethylene from the complicated mixtures, indicating its excellent capability for the purification of ethylene.

Very recently, Zhang and coworkers reported full separation of ethane and ethylene by a HOF material through a gating mechanism.<sup>107</sup> The material, HOF-FJU-1, was constructed from a tetracyano-bicarbazole building block, which possessed permanent porosity and flexible framework. As a result of the structure flexibility, the adsorption of ethane and ethylene on HOF-FJU-1 exhibited a gating behavior and was highly temperature-dependent. At 318 and 333 K, it adsorbs ethylene only and fully excluded ethane, showing a molecular sieving behavior. Column breakthrough measurements confirmed the capability of HOF-FJU-1 for the capture of ethylene from a

mixture of ethylene, ethane, propylene, propane, methane, and hydrogen.

## 5. Conclusion and outlook

In this review, we provide an overview of the major advancement in  $C_2$ - $C_3$  alkane/alkene separation by metal-organic frameworks. We present the research progress based on three separation mechanisms: thermodynamic separation (including alkane-selective and alkene-selective), kinetic separation, and selective size exclusion-based separation. Representative examples in each category are discussed and material design strategies and structure-property relationship are emphasized. It is exciting to witness the tremendous progresses in developing tailored MOFs for highly efficient separation of alkanes and alkenes over the past a few years, particular those of alkane-selective MOFs with relatively high adsorption selectivity. In addition, several MOFs that are capable of separating alkane and alkene via selective molecular exclusion have been achieved through rational design. These achievements demonstrate that MOFs are indeed promising adsorbent materials for the separation of alkanes/alkenes. Some of them have already outperformed traditional adsorbents for certain separation processes.

The potential of MOFs for alkane/alkene separation has been well illustrated in this review article. However, some concerns and challenges need to be addressed in the future development of MOFs for their implementation in industries: 1) Material stability. MOFs have suffered from relatively poor stability compared to conventional inorganic adsorbents since they first emerged. This issue has been partially addressed over the past decade by various approaches, such as the incorporation of early transition metals as inorganic building units. Some of the MOFs presented in this article are sensitive to moisture or air, which limits their application even though they may have excellent separation performance. Material stability and long-term durability would be the primary aspect to consider for developing MOFs for industrial applications. In addition to thermal and moisture stability, their resistance to other gaseous impurities that are present in the stream should be assessed. For example, Eddaoudi et al. evaluated the stability of KAUST-7 under  $H_2S$  exposure when exploring its potential for propane/propylene separation.<sup>13</sup> Similar experiments are recommended for all adsorbents that are aimed for alkane/alkene separation applications. 2) Trade-off between adsorption capacity and selectivity. It is noteworthy from the overview in this article that some MOFs have either high adsorption capacity or adsorption selectivity for alkane/alkene separation, but seldomly have both. For example, the adsorption capacities for those showing selective molecular exclusion are typically low. A way to potentially resolve this issue is to rely on the rational design of materials. Reticular chemistry can guide the researchers to precisely control the resulting structures with an ideal topology/pore structure or to

introduce an optimal adsorption site. 3) Evaluation conditions. Practical conditions of alkane/alkene separation may differ, depending on the source of feed mixtures. For example, propane/propylene mixtures from steam cracking of naphtha are usually equimolar, while the mixture from fluid catalytic cracking has 80+% propylene. Thus, for a specific separation process it is important to determine whether alkane-selective or alkene-selective adsorbents is preferred and the optimal conditions for the adsorbent. Moreover, the adsorption and separation capability of MOFs should be evaluated under industrially relevant conditions including other minor components likely to be present in industrial scenario, rather than a mixture of pure olefin and paraffin. 4) Cost. Comparing with conventional adsorbent materials, the syntheses of MOFs are generally more expensive, especially when large, complex organic linkers are involved. Future endeavours in making cost effective yet highly robust MOFs with desirable porosity using inexpensive ligands are much needed for real-world applications.

Effective separation of alkanes and alkenes is of paramount importance in petrochemical industry for various uses, for example, to produce high purity ethylene and propylene. These processes currently rely on cryogenic distillation, suggesting that ideal adsorbents for adsorptive separation are yet to be developed. To the best of our knowledge, neither zeolites nor MOFs have been used for industrial separation of alkane and alkene so far. However, they are the current research focus in scientific community and represent two most promising types of adsorbents that may become suitable candidates for industrial implementation. Zeolites are well-explored, highly stable, and relatively inexpensive. On the other hand, MOFs are a relatively new adsorbent class with numerous advantages. The exploration of MOFs for adsorptive alkane/alkene separation is undergoing a very rapid growth. Although challenges remain for the industrial implementation of MOFs, including stability, cost, etc., their exceptionally tunable structure and pore geometry/size, and diverse gas-framework interactions make them highly valuable for both fundamental research and industrial applications. While some of the challenges may be difficult to overcome, with the tireless efforts of many researchers working in the field, we are confident that great advancement will continue to be made and the future is bright for the development of MOF-based adsorbents suitable for separation of alkanes and alkenes.

## Conflicts of interest

There are no conflicts to declare.

## Acknowledgements

We thank the National Natural Science Foundation of China (No. 21901166), Natural Science Foundation of Guangdong Province (No. 2019A1515010692), Shenzhen Science and Technology

Program (No. JCYJ20190809145615620, RCYX20200714114539243) and the U. S. Department of Energy, Office of Science, Office of Basic Energy Sciences (DE-SC0019902) for the financial support.

## Notes and references

‡ Footnotes relating to the main text should appear here. These might include comments relevant not central to the matter under discussion, limited experimental and spectral data, and crystallographic data.

- R. A. Myers, *Handbook of Petroleum Refining Processes*, McGraw-Hill, New York, 2004.
- R. Lively, *Nature*, 2016, **532**, 435-437.
- P. J. Bereciartua, Á. Cantín, A. Corma, J. L. Jordá, M. Palomino, F. Rey, S. Valencia, E. W. Corcoran, P. Kortunov, P. I. Ravikovitch, A. Burton, C. Yoon, Y. Wang, C. Paur, J. Guzman, A. R. Bishop and G. L. Casty, *Science*, 2017, **358**, 1068.
- Y. Liu, Y. Wu, W. Liang, J. Peng, Z. Li, H. Wang, M. J. Janik and J. Xiao, *Chemical Engineering Science*, 2020, **220**, 115636.
- D. Saha, B. Toof, R. Krishna, G. Orkoulas, P. Gismond, R. Thorpe and M. L. Comroe, *Microporous and Mesoporous Materials*, 2020, **299**, 110099.
- P. Zhang, X. Wen, L. Wang, Y. Zhong, Y. Su, Y. Zhang, J. Wang, J. Yang, Z. Zeng and S. Deng, *Chemical Engineering Journal*, 2020, **381**, 122731.
- C. Yu, M. G. Cowan, R. D. Noble and W. Zhang, *Chemical Communications*, 2014, **50**, 5745-5747.
- L. Huang and D. Cao, *Journal of Materials Chemistry A*, 2013, **1**, 9433-9439.
- B. Li, Y. Zhang, R. Krishna, K. Yao, Y. Han, Z. Wu, D. Ma, Z. Shi, T. Pham, B. Space, J. Liu, P. K. Thallapally, J. Liu, M. Chrzanoski and S. Ma, *Journal of the American Chemical Society*, 2014, **136**, 8654-8660.
- M. C. Campo, A. M. Ribeiro, A. Ferreira, J. C. Santos, C. Lutz, J. M. Loureiro and A. E. Rodrigues, *Separation and Purification Technology*, 2013, **103**, 60-70.
- J. Gi Min, K. Christian Kemp, K. S. Kencana, R. R. Mukti and S. Bong Hong, *Chemical Engineering Journal*, 2021, **413**, 127422.
- M. Khalighi, I. A. Karimi and S. Farooq, *Industrial & Engineering Chemistry Research*, 2014, **53**, 16973-16983.
- A. Cadiau, K. Adil, P. M. Bhatt, Y. Belmabkhout and M. Eddaoudi, *Science*, 2016, **353**, 137.
- H. Wang, Y. Liu and J. Li, *Advanced Materials*, 2020, **32**, 2002603.
- W.-G. Cui, T.-L. Hu and X.-H. Bu, *Advanced Materials*, 2020, **32**, 1806445.
- J. Pei, K. Shao, L. Zhang, H.-M. Wen, B. Li and G. Qian, *Topics in Current Chemistry*, 2019, **377**, 33.
- K. Adil, Y. Belmabkhout, R. S. Pillai, A. Cadiau, P. M. Bhatt, A. H. Assen, G. Maurin and M. Eddaoudi, *Chemical Society Reviews*, 2017, **46**, 3402-3430.
- Z. R. Herm, E. D. Bloch and J. R. Long, *Chemistry of Materials*, 2014, **26**, 323-338.
- Z. Bao, G. Chang, H. Xing, R. Krishna, Q. Ren and B. Chen, *Energy & Environmental Science*, 2016, **9**, 3612-3641.
- L. Li, R.-B. Lin, R. Krishna, H. Li, S. Xiang, H. Wu, J. Li, W. Zhou and B. Chen, *Science*, 2018, **362**, 443.
- R.-B. Lin, L. Li, H.-L. Zhou, H. Wu, C. He, S. Li, R. Krishna, J. Li, W. Zhou and B. Chen, *Nature Materials*, 2018, **17**, 1128-1133.
- T. M. Nicholson and S. K. Bhatia, *The Journal of Physical Chemistry B*, 2006, **110**, 24834-24836.
- T. M. Nicholson and S. K. Bhatia, *Adsorption Science & Technology*, 2007, **25**, 607-619.
- S. Wang, Q. Yang and C. Zhong, *Separation and Purification Technology*, 2008, **60**, 30-35.
- , !!! INVALID CITATION !!! 4, 5.
- Y. Sun, Z. Ke, Y. Tang, S. Wang, Y. Wu, Q. Xia and Z. Li, *Industrial & Engineering Chemistry Research*, 2020, **59**, 6202-6209.
- J. W. Yoon, Y.-K. Seo, Y. K. Hwang, J.-S. Chang, H. Leclerc, S. Wuttke, P. Bazin, A. Vimont, M. Daturi, E. Bloch, P. L. Llewellyn, C. Serre, P. Horcajada, J.-M. Grenèche, A. E. Rodrigues and G. Férey, *Angewandte Chemie International Edition*, 2010, **49**, 5949-5952.
- Y.-S. Bae, C. Y. Lee, K. C. Kim, O. K. Farha, P. Nickias, J. T. Hupp, S. T. Nguyen and R. Q. Snurr, *Angewandte Chemie International Edition*, 2012, **51**, 1857-1860.
- Z. Bao, S. Alnemrat, L. Yu, I. Vasiliev, Q. Ren, X. Lu and S. Deng, *Langmuir*, 2011, **27**, 13554-13562.
- E. D. Bloch, W. L. Queen, R. Krishna, J. M. Zadrozny, C. M. Brown and J. R. Long, *Science*, 2012, **335**, 1606.
- S. J. Geier, J. A. Mason, E. D. Bloch, W. L. Queen, M. R. Hudson, C. M. Brown and J. R. Long, *Chemical Science*, 2013, **4**, 2054-2061.
- J. E. Bachman, M. T. Kapelewski, D. A. Reed, M. I. Gonzalez and J. R. Long, *Journal of the American Chemical Society*, 2017, **139**, 15363-15370.
- G. Chang, M. Huang, Y. Su, H. Xing, B. Su, Z. Zhang, Q. Yang, Y. Yang, Q. Ren, Z. Bao and B. Chen, *Chemical Communications*, 2015, **51**, 2859-2862.
- L. Zhang, L. Li, E. Hu, L. Yang, K. Shao, L. Yao, K. Jiang, Y. Cui, Y. Yang, B. Li, B. Chen and G. Qian, *Advanced Science*, 2020, **7**, 1901918.
- X. Wang, P. Zhang, Z. Zhang, L. Yang, Q. Ding, X. Cui, J. Wang and H. Xing, *Industrial & Engineering Chemistry Research*, 2020, **59**, 3531-3537.
- S. Yang, A. J. Ramirez-Cuesta, R. Newby, V. Garcia-Sakai, P. Manuel, S. K. Callear, S. I. Campbell, C. C. Tang and M. Schröder, *Nature Chemistry*, 2015, **7**, 121-129.
- X. Wang, R. Krishna, L. Li, B. Wang, T. He, Y.-Z. Zhang, J.-R. Li and J. Li, *Chemical Engineering Journal*, 2018, **346**, 489-496.
- K.-J. Chen, D. G. Madden, S. Mukherjee, T. Pham, K. A. Forrest, A. Kumar, B. Space, J. Kong, Q.-Y. Zhang and M. J. Zaworotko, *Science*, 2019, **366**, 241.
- , !!! INVALID CITATION !!! 10, 11.
- M. Hartmann, U. Böhme, M. Hovestadt and C. Paula, *Langmuir*, 2015, **31**, 12382-12389.
- A.-R. Kim, T.-U. Yoon, E.-J. Kim, J. W. Yoon, S.-Y. Kim, J. W. Yoon, Y. K. Hwang, J.-S. Chang and Y.-S. Bae, *Chemical Engineering Journal*, 2018, **331**, 777-784.
- Y. Chen, H. Wu, D. Lv, N. Yuan, Q. Xia and Z. Li, *Separation and Purification Technology*, 2018, **204**, 75-80.
- S.-Y. Kim, T.-U. Yoon, J. H. Kang, A.-R. Kim, T.-H. Kim, S.-I. Kim, W. Park, K. C. Kim and Y.-S. Bae, *ACS Applied Materials & Interfaces*, 2018, **10**, 27521-27530.
- Z. Chang, R.-B. Lin, Y. Ye, C. Duan and B. Chen, *Journal of Materials Chemistry A*, 2019, **7**, 25567-25572.

45. L. Yang, X. Cui, Q. Ding, Q. Wang, A. Jin, L. Ge and H. Xing, *ACS Applied Materials & Interfaces*, 2020, **12**, 2525-2530.
46. C. He, Y. Wang, Y. Chen, X. Wang, J. Yang, L. Li and J. Li, *Chemical Engineering Journal*, 2021, **403**, 126428.
47. S. Wang, Y. Zhang, Y. Tang, Y. Wen, Z. Lv, S. Liu, X. Li and X. Zhou, *Chemical Engineering Science*, 2020, **219**, 115604.
48. U. Böhme, B. Barth, C. Paula, A. Kuhnt, W. Schwieger, A. Mundstock, J. Caro and M. Hartmann, *Langmuir*, 2013, **29**, 8592-8600.
49. H. Bigdelou, M. R. Khosravi-Nikou and A. Shariati, *Chemical Engineering Research and Design*, 2020, **159**, 315-327.
50. H. Xiang, A. Ameen, J. Shang, Y. Jiao, P. Gorgojo, F. R. Siperstein and X. Fan, *Microporous and Mesoporous Materials*, 2020, **293**, 109784.
51. Y. Yin, Z. Zhang, C. Xu, H. Wu, L. Shi, S. Wang, X. Xu, A. Yuan, S. Wang and H. Sun, *ACS Sustainable Chemistry & Engineering*, 2020, **8**, 823-830.
52. Y. Wang, S. Yuan, Z. Hu, T. Kundu, J. Zhang, S. B. Peh, Y. Cheng, J. Dong, D. Yuan, H.-C. Zhou and D. Zhao, *ACS Sustainable Chemistry & Engineering*, 2019, **7**, 7118-7126.
53. L. Li, L. Guo, S. Pu, J. Wang, Q. Yang, Z. Zhang, Y. Yang, Q. Ren, S. Alnemrat and Z. Bao, *Chemical Engineering Journal*, 2019, **358**, 446-455.
54. Y. Wang, Z. Hu, Y. Cheng and D. Zhao, *Industrial & Engineering Chemistry Research*, 2017, **56**, 4508-4516.
55. K. H. Cho, J. W. Yoon, J. H. Lee, J. C. Kim, K. Kim, U. H. Lee, S. K. Kwak and J.-S. Chang, *Microporous and Mesoporous Materials*, 2020, **307**, 110473.
56. X.-W. Lei, H. Yang, Y. Wang, Y. Wang, X. Chen, Y. Xiao, X. Bu and P. Feng, *Small*, 2020, **n/a**, 2003167.
57. A. A. Lysova, D. G. Samsonenko, K. A. Kovalenko, A. S. Nizovtsev, D. N. Dybtsev and V. P. Fedin, *Angewandte Chemie International Edition*, 2020, **59**, 20561-20567.
58. O. T. Qazvini, L. K. Macreadie and S. G. Telfer, *Chemistry of Materials*, 2020, **32**, 6744-6752.
59. O. T. Qazvini, R. Babarao, Z.-L. Shi, Y.-B. Zhang and S. G. Telfer, *Journal of the American Chemical Society*, 2019, **141**, 5014-5020.
60. Y. Lin, Y. Li, H. Wang, D. Luo, F. Lin and J. Li, *New Journal of Chemistry*, 2020, **44**, 11933-11936.
61. H. Xiang, Y. Shao, A. Ameen, H. Chen, W. Yang, P. Gorgojo, F. R. Siperstein, X. Fan and Q. Pan, *Separation and Purification Technology*, 2020, **242**, 116819.
62. A. Dinh, H. Yang, F. Peng, T. C. Nguyen, A. Hong, P. Feng and X. Bu, *Crystal Growth & Design*, 2020, **20**, 3523-3530.
63. C. He, Y. Wang, Y. Chen, X. Wang, J. Yang, L. Li and J. Li, *Industrial & Engineering Chemistry Research*, 2020, **59**, 6123-6129.
64. L. Yang, Y. Wang, Y. Chen, J. Yang, X. Wang, L. Li and J. Li, *Chemical Engineering Journal*, 2020, **387**, 124137.
65. Y. Tang, S. Wang, X. Zhou, Y. Wu, S. Xian and Z. Li, *Chemical Engineering Science*, 2020, **213**, 115355.
66. R.-B. Lin, H. Wu, L. Li, X.-L. Tang, Z. Li, J. Gao, H. Cui, W. Zhou and B. Chen, *Journal of the American Chemical Society*, 2018, **140**, 12940-12946.
67. F.-Z. Sun, S.-Q. Yang, R. Krishna, Y.-H. Zhang, Y.-P. Xia and T.-L. Hu, *ACS Applied Materials & Interfaces*, 2020, **12**, 6105-6111.
68. J. Pei, J.-X. Wang, K. Shao, Y. Yang, Y. Cui, H. Wu, W. Zhou, B. Li and G. Qian, *Journal of Materials Chemistry A*, 2020, **8**, 3613-3620.
69. L. Yang, W. Zhou, H. Li, A. Alsalmeh, L. Jia, J. Yang, J. Li, L. Li and B. Chen, *Chinese Journal of Chemical Engineering*, 2020, **28**, 593-597.
70. H. Yang, Y. Wang, R. Krishna, X. Jia, Y. Wang, A. N. Hong, C. Dang, H. E. Castillo, X. Bu and P. Feng, *Journal of the American Chemical Society*, 2020, **142**, 2222-2227.
71. H. Xiang, A. Ameen, P. Gorgojo, F. R. Siperstein, S. M. Holmes and X. Fan, *Microporous and Mesoporous Materials*, 2020, **292**, 109724.
72. W. Liang, F. Xu, X. Zhou, J. Xiao, Q. Xia, Y. Li and Z. Li, *Chemical Engineering Science*, 2016, **148**, 275-281.
73. H. Zeng, X.-J. Xie, M. Xie, Y.-L. Huang, D. Luo, T. Wang, Y. Zhao, W. Lu and D. Li, *Journal of the American Chemical Society*, 2019, **141**, 20390-20396.
74. D. Lv, J. Chen, Y. Chen, Z. Liu, Y. Xu, C. Duan, H. Wu, Y. Wu, J. Xiao, H. Xi, Z. Li and Q. Xia, *AIChE Journal*, 2019, **65**, e16616.
75. J. Pires, J. Fernandes, K. Dedecker, J. R. B. Gomes, G. Pérez-Sánchez, F. Nouar, C. Serre and M. L. Pinto, *ACS Applied Materials & Interfaces*, 2019, **11**, 27410-27421.
76. H. Wu, Y. Chen, W. Yang, D. Lv, Y. Yuan, Z. Qiao, H. Liang, Z. Li and Q. Xia, *Industrial & Engineering Chemistry Research*, 2019, **58**, 10516-10523.
77. X. Wang, Z. Niu, A. M. Al-Enizi, A. Nafady, Y. Wu, B. Aguila, G. Verma, L. Wojtas, Y.-S. Chen, Z. Li and S. Ma, *Journal of Materials Chemistry A*, 2019, **7**, 13585-13590.
78. H. Wu, Y. Chen, D. Lv, R. Shi, Y. Chen, Z. Li and Q. Xia, *Separation and Purification Technology*, 2019, **212**, 51-56.
79. Y. Chen, H. Wu, D. Lv, R. Shi, Y. Chen, Q. Xia and Z. Li, *Industrial & Engineering Chemistry Research*, 2018, **57**, 4063-4069.
80. D. Lv, R. Shi, Y. Chen, Y. Wu, H. Wu, H. Xi, Q. Xia and Z. Li, *ACS Applied Materials & Interfaces*, 2018, **10**, 8366-8373.
81. Y. Chen, Z. Qiao, H. Wu, D. Lv, R. Shi, Q. Xia, J. Zhou and Z. Li, *Chemical Engineering Science*, 2018, **175**, 110-117.
82. W. Yuan, X. Zhang and L. Li, *Journal of Solid State Chemistry*, 2017, **251**, 198-203.
83. P.-Q. Liao, W.-X. Zhang, J.-P. Zhang and X.-M. Chen, *Nature Communications*, 2015, **6**, 8697.
84. J. Pires, M. L. Pinto and V. K. Saini, *ACS Applied Materials & Interfaces*, 2014, **6**, 12093-12099.
85. C. Gücüyener, J. van den Bergh, J. Gascon and F. Kapteijn, *Journal of the American Chemical Society*, 2010, **132**, 17704-17706.
86. E. D. Bloch, L. J. Murray, W. L. Queen, S. Chavan, S. N. Maximoff, J. P. Bigi, R. Krishna, V. K. Peterson, F. Grandjean, G. J. Long, B. Smit, S. Bordiga, C. M. Brown and J. R. Long, *Journal of the American Chemical Society*, 2011, **133**, 14814-14822.
87. H. Xiang, X. Fan and F. R. Siperstein, *Separation and Purification Technology*, 2020, **241**, 116635.
88. H. Tang and J. Jiang, *AIChE Journal*, 2021, **67**, e17025.
89. C. He, Y. Wang, Y. Chen, X. Wang, J. Yang, L. Li and J. Li, *ACS Applied Materials & Interfaces*, 2020, **12**, 52819-52825.
90. X. Zhang, J.-X. Wang, L. Li, J. Pei, R. Krishna, H. Wu, W. Zhou, G. Qian, B. Chen and B. Li, *Angewandte Chemie International Edition*, 2021, **60**, 10304-10310.
91. X. Zhang, L. Li, J.-X. Wang, H.-M. Wen, R. Krishna, H. Wu, W. Zhou, Z.-N. Chen, B. Li, G. Qian and B. Chen, *Journal of the American Chemical Society*, 2020, **142**, 633-640.
92. K. Li, D. H. Olson, J. Seidel, T. J. Emge, H. Gong, H. Zeng and

- J. Li, *Journal of the American Chemical Society*, 2009, **131**, 10368-10369.
93. C. Y. Lee, Y.-S. Bae, N. C. Jeong, O. K. Farha, A. A. Sarjeant, C. L. Stern, P. Nickias, R. Q. Snurr, J. T. Hupp and S. T. Nguyen, *Journal of the American Chemical Society*, 2011, **133**, 5228-5231.
94. J. Peng, H. Wang, D. H. Olson, Z. Li and J. Li, *Chemical Communications*, 2017, **53**, 9332-9335.
95. D.-X. Xue, A. Cadiau, Ł. J. Weseliński, H. Jiang, P. M. Bhatt, A. Shkurenko, L. Wojtas, C. Zhijie, Y. Belmabkhout, K. Adil and M. Eddaoudi, *Chemical Communications*, 2018, **54**, 6404-6407.
96. L. Li, R.-B. Lin, X. Wang, W. Zhou, L. Jia, J. Li and B. Chen, *Chemical Engineering Journal*, 2018, **354**, 977-982.
97. Y. Wang, N.-Y. Huang, X.-W. Zhang, H. He, R.-K. Huang, Z.-M. Ye, Y. Li, D.-D. Zhou, P.-Q. Liao, X.-M. Chen and J.-P. Zhang, *Angewandte Chemie International Edition*, 2019, **58**, 7692-7696.
98. H. Wu, Y. Yuan, Y. Chen, F. Xu, D. Lv, Y. Wu, Z. Li and Q. Xia, *AIChE Journal*, 2020, **66**, e16858.
99. Q. Ding, Z. Zhang, C. Yu, P. Zhang, J. Wang, L. Kong, X. Cui, C.-H. He, S. Deng and H. Xing, *AIChE Journal*, 2021, **67**, e17094.
100. R. Lyndon, W. You, Y. Ma, J. Bacsá, Y. Gong, E. E. Stangland, K. S. Walton, D. S. Sholl and R. P. Lively, *Chemistry of Materials*, 2020, **32**, 3715-3722.
101. C. Gu, N. Hosono, J.-J. Zheng, Y. Sato, S. Kusaka, S. Sakaki and S. Kitagawa, *Science*, 2019, **363**, 387.
102. Q. Ding, Z. Zhang, C. Yu, P. Zhang, J. Wang, X. Cui, C.-H. He, S. Deng and H. Xing, *Science Advances*, 2020, **6**, eaaz4322.
103. H. Wang, X. Dong, V. Colombo, Q. Wang, Y. Liu, W. Liu, X.-L. Wang, X.-Y. Huang, D. M. Proserpio, A. Sironi, Y. Han and J. Li, *Advanced Materials*, 2018, **30**, 1805088.
104. B. Liang, X. Zhang, Y. Xie, R.-B. Lin, R. Krishna, H. Cui, Z. Li, Y. Shi, H. Wu, W. Zhou and B. Chen, *Journal of the American Chemical Society*, 2020, **142**, 17795-17801.
105. Z. Bao, J. Wang, Z. Zhang, H. Xing, Q. Yang, Y. Yang, H. Wu, R. Krishna, W. Zhou, B. Chen and Q. Ren, *Angewandte Chemie International Edition*, 2018, **57**, 16020-16025.
106. C. Robl and A. Weiss, *Materials Research Bulletin*, 1987, **22**, 373-380.
107. Y. Yang, L. Li, R.-B. Lin, Y. Ye, Z. Yao, L. Yang, F. Xiang, S. Chen, Z. Zhang, S. Xiang and B. Chen, *Nature Chemistry*, 2021, DOI: 10.1038/s41557-021-00740-z.



